JACS
JOURNAL OF THE AMERICAN CHEMICAL SOCIETY
Article
pubs.acs.org/JACS

Atomistic Description of Thiostannate-Capped CdSe Nanocrystals: Retention of Four-Coordinate SnS4 Motif and Preservation of Cd-Rich Stoichiometry

Loredana Protesescu,[†,‡] Maarten Nachtegaal,[∥] Oleksandr Voznyy,[⊥] Olga Borovinskaya,[†] Aaron J. Rossini,[§] Lyndon Emsley,[§] Christophe Copéret,[†] Detlef Günther,[†] Edward H. Sargent,[⊥] and Maksym V. Kovalenko*[,†,‡]

[†]Institute of Inorganic Chemistry, Department of Chemistry and Applied Biosciences, ETH Zürich, Vladimir Prelog Weg 1, Zurich CH-8093, Switzerland

[‡]Empa-Swiss Federal Laboratories for Materials Science and Technology, Überlandstrasse 129, Dübendorf CH-8600, Switzerland

[§]Centre de RMN à Trés Hauts Champs, Institut de Sciences Analytiques (CNRS/ENS Lyon/UCB Lyon 1), Université de Lyon, 69100 Villeurbanne, France

[∥]Paul Scherrer Institute, 5232 Villigen PSI, Switzerland

[⊥]Department of Electrical and Computer Engineering, University of Toronto, 10 King's College Road, Toronto, Ontario M5S 3G4, Canada

Supporting Information

ABSTRACT: Colloidal semiconductor nanocrystals (NCs) are widely studied as building blocks for novel solid-state materials. Inorganic surface functionalization, used to displace native organic capping ligands from NC surfaces, has been a major enabler of electronic solid-state devices based on colloidal NCs. At the same time, very little is known about the atomistic details of the organic-to-inorganic ligand exchange and binding motifs at the NC surface, severely limiting further progress in designing all-inorganic NCs and NC solids. Taking thiostannates (K_4SnS_4, $K_4Sn_2S_6$, $K_6Sn_2S_7$) as typical examples of chalcogenidometallate ligands and oleate-capped CdSe NCs as a model NC system, in this study we address these questions through the combined application of solution ^1H NMR spectroscopy, solution and solid-state ^{119}Sn NMR spectroscopy, far-infrared and X-ray absorption spectroscopies, elemental analysis, and by DFT modeling. We show that through the X-type oleate-to-thiostannate ligand exchange, CdSe NCs retain their Cd-rich stoichiometry, with a stoichiometric CdSe core and surface Cd adatoms serving as binding sites for terminal S atoms of the thiostannates ligands, leading to all-inorganic $(CdSe)_{core}[Cd_m(Sn_2S_7)_yK_{(6y-2m)}]_{shell}$ (taking $Sn_2S_7^{6-}$ ligand as an example). Thiostannates SnS_4^{4-} and $Sn_2S_7^{6-}$ retain (distorted) tetrahedral SnS_4 geometry upon binding to NC surface. At the same time, experiments and simulations point to lower stability of $Sn_2S_6^{4-}$ (and SnS_3^{2-}) in most solvents and its lower adaptability to the NC surface caused by rigid Sn_2S_2 rings.

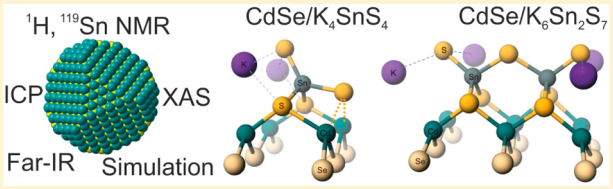

INTRODUCTION

In a nonvacuum environment, metal ions and atoms do not exist in a completely isolable form but in a solvated or ligand-coordinated state. Similarly, inorganic nanoparticles or nanocrystals (NCs, crystalline nanoparticles) require a shell of capping molecules, also known as ligands, to ensure their chemical and colloidal stability. Proper selection of organic surface capping ligands, such as long-chain organic molecules with a metal binding functional headgroup, has enabled the development of monodisperse colloidal NCs since the early 1990s.[1] Capping ligands also largely dictate the individual physical and chemical properties of NCs, as well as the collective electronic properties in the densely packed NC solids.[1a,2] Owing to the highly insulating character of commonly used long-chain capping ligands, novel chemistries based on short-chain and conductive ligands, organic or inorganic, were required for demonstration of NC-based solar cells,[3] light-emitting diodes,[4] photodetectors,[5] thermoelectrics,[6] transistors,[5c,7] and integrated electronic circuits.[8] In this regard, colloidally stable, all-inorganic NCs are readily obtained by solution-phase exchange of organic ligands with common inorganic anions such as metal chalcogenide complexes (MCCs, also known as chalcogenidometallates),[9] metal-free ions (S^{2-}, HS^-, Se^{2-}, OH^-, SCN^-, I^-, etc.),[7,8b,10] oxo- and polyoxometallates,[11] and metal halide complexes (halometallates).[10c,12] In addition, a powerful and complementary methodology is the formation of cationic and naked, but colloidally stable, NCs upon controlled stripping of the strongly bound native organic ligands with the simultaneous coordination of

Received: October 24, 2014
Published: January 17, 2015

DOI: 10.1021/ja510862c
J. Am. Chem. Soc. 2015, 137, 1862−1874

metal cations on the NC surface with weakly nucleophilic ligands.[13]

Overall, the inorganic surface functionalization of semiconductor NCs has been the major enabler of NC-based electronic and optoelectronic devices in the last 5 years. Thus far, particularly efficient inorganic ligands, in terms of the speed of ligand-exchange (LE) reactions, affinity to and compatibility with various NCs, have been MCCs due to the high affinity of terminal chalcogen atoms to undercoordinated metal atoms on the NC surface. In highly polar solvents, such as water or methylformamide (MFA), these NCs are electrostatically stabilized due to adsorption of anionic ligands onto the NC surface and electrostatic dissociation of the counterions. Not only are the integrity and size-tunable optical properties of NCs fully preserved, but also the charge transport in the solids comprising such all-inorganic NCs is greatly improved, and electronic mobilities of 5−35 $cm^2\ V^{-1}\ s^{-1}$ are now routinely obtained.[7,8,14] Additionally, these all-inorganic colloids of semiconductor NCs have enabled photodetectors with detectivities of up to 10^{13} Jones,[15] improved electrocatalytic properties of CdSe NCs (hydrogen evolution),[16] and enhanced electronic transport in NC-based Li-ion batteries.[17] Inorganic-capped NCs have also served as fully inorganic inks for solution-deposited $CuInS_2$, $Cu(In_{1-x}Ga_x)Se_2$, $Cu_2ZnSn(S,Se)_4$ (CZTS), and PbS phases as thin-film absorbers for photovoltaics,[18] ionically conductive composites of Ag_2S NCs embedded into a GeS_2 matrix,[19] or Sb_2Te_3-based nanocomposites for thermoelectrics;[6a,d] for integration of highly luminescent PbS/CdS NCs into fully inorganic infrared-transparent matrices;[20] and for design of NC-in-glass windows with electrochemically tunable transmittance.[11a,21] Solution-phase or solid-state preparation of NCs with either partial or full surface coverage by halide ions has also been reported by several groups.[22] Halide ion ligands provide improved electronic passivation of semiconductor NCs, high oxidative stability, and power conversion efficiencies of up to 8.6% in PbS NC-based photovoltaics.[23]

The aforementioned superior electrical characteristics of the solids composed of inorganically capped NCs have stimulated this study. Here, we aim to better understand the underlying chemistry of the organic-to-inorganic LE and to unveil the atomistic ligand bonding motifs. Contrary to very successful recent studies on the atomistic details of organic ligand capping,[22f,h,24] so far no systematic and direct spectroscopic studies, and atomistic simulations of the inorganic surface capping and LE reactions with complex ions such as chalcogenidometalates, have been reported. The completeness of the removal of initial organic ligands as well as the presence of smaller, inorganic capping species was mainly judged from indirect observations such as diminishing of the C−H stretching modes in FTIR spectra, solubility in polar solvents and electrophoretic mobility measurements, elemental analysis, increased electronic coupling, and decreased interparticle spacing in NC solids. These techniques, however, do not provide direct information about the chemical identity of the surface-bound species and do not probe local binding motifs at the NC surface. Only one recent direct spectroscopic study had dealt with smaller thiocyanate-ligands and confirmed the formation of chemical bonds between inorganic ligands and the NC surface (FTIR spectra of the metal- inorganic ligand bonds at the surface).[10d] In contrast with thiocyanates, MCC ligands have a higher affinity for NC surfaces and are capable of multidentate bonding. The lack of knowledge about the mechanism of the LE reactions with MCCs and other inorganic ligands hinders the rational design of new materials and our ability to further tune their electronic and optical characteristics.

An atomically precise image of the NC surface is not yet available, nor are the NCs surfaces atomically precise and static. Faceting, surface reconstructions, and the dynamic nature of these phenomena complicate the task.[24] Furthermore, the techniques that are used to determine the atomic coordinates in crystalline inorganic materials are inherently blind to the surfaces (e.g., X-ray or electron diffraction). Therefore, building the atomistic picture of ligand-capped NCs requires a powerful combination of modern experimental tools and atomistic modeling. In this study, several experimental techniques (nuclear magnetic resonance, X-ray absorption, Raman and far-infrared spectroscopies, and elemental analysis) were combined with atomistic simulations at density functional theory level (DFT) in order to understand the LE reactions involving carboxylate-capped CdSe NCs and thiostannate ligands ($Sn_2S_6^{4-}$, $Sn_2S_7^{6-}$, SnS_4^{4-}). Our study has concentrated on these air-stable, sulfide-based ligands to minimize the effects caused by the degradation of the ligands. The majority of results concern Sn−S MCCs, due to high suitability of the ^{119}Sn isotope for solution and solid-state NMR studies and because we also wanted to shed light onto the solution-based equilibria between several Sn−S ligands. In particular, ^{119}Sn solution NMR spectroscopy allowed us to identify the ligands and their equilibria in various solvents, while ^{119}Sn solid-state NMR provides insight into their surface-bound state. CdSe NCs serve as a convenient model NC system due to extensive prior work on their synthesis, surface chemistry, and photophysics. In particular, carboxylate-capped CdSe NCs were previously shown to consist of a stoichiometric CdSe core covered with a layer of $Cd(O_2CR)_2$.[22f−h] Thus, an important question specific to LE with MCCs is whether carboxylate is replaced as an anionic moiety (X-type exchange) or is detached as molecular complex $Cd(O_2CR)_2$.

The key findings of this study are as follows. First, we identify the presence of $Sn_2S_7^{6-}$ ions and their role as a predominant form of thiostannate in *N*-methylformamide (MFA). Second, the LE reaction with all studied thiostannate and other MCC ligands retains the Cd-rich stoichiometry of CdSe NC surface, with a purely X-type displacement of the initial oleate ligand. This study also compares relative binding strengths of MCC ligands and simple S^{2-} ions, including several MCCs that had not been used as capping ligands before (GeS_4^{4-}, SbS_4^{3-}, and $Sn_2S_7^{6-}$). Thiostannate ligands SnS_4^{4-}, $Sn_2S_6^{4-}$, and $Sn_2S_7^{6-}$ convert into each other upon dissolution in various solvents, pointing to the importance of solution equilibra. Thiostannate ions largely maintain a tetrahedral SnS_4 motif after the binding to the NC surface. The multidentate nature of MCCs allows a broad spectrum of binding modes. Atomistic simulations support this observation and suggest polydentate binding of SnS_4^{4-} and $Sn_2S_7^{6-}$ ions as most plausible forms of Sn−S adsorbates on CdSe NC surfaces. Finally, atomistic simulations also corroborate previously reported optical and charge transport measurements, showing the key role played by the ligand in quenching the photoluminescence and for stable n-type doping. Knowledge obtained for CdSe−thiostannate system may shed light onto behavior of other technologically important NC−MCC systems.

DOI: 10.1021/ja510862c
J. Am. Chem. Soc. 2015, 137, 1862−1874

EXPERIMENTAL SECTION

Materials. Selenium dioxide (SeO_2, 99.9+%, Strem), oleic acid (OA, 90%, Aldrich), 1-octadecene (ODE, 90%, Aldrich), methanol (Aldrich, 98%), cadmium nitrate tetrahydrate ($Cd(NO_3)_2 \times 4H_2O$, 99.99%, Aldrich), CdO (99.99+, Sigma-Aldrich), myristic acid (MA, 99%, Aldrich), sodium hydroxide (NaOH, Aldrich), hexane (>95% Sigma-Aldrich), ethanol (99.8%, Fluka), toluene (99%, Fischer), formamide (FA, 99.5+%, Aldrich), acetonitrile (MeCN, 99.9%, Sigma-Aldrich), *N*-methyl formamide (MFA, 99%, Aldrich), dimethylformamide (DMF, 99.8%, Sigma-Aldrich), hydrazine (98%, anhydrous, Aldrich), potassium sulfide (K_2S, 99.5%, Strem), ammonium sulfide (40−48% solution in water, Aldrich), antimony(III) sulfide (Sb_2S_3, 99.995%, Aldrich), germanium(II) sulfide (GeS, 99.99%, Aldrich), sulfur (99.998%, Sigma-Aldrich), As_2S_5 (99.99%, Sigma-Aldrich), triethyloxonium tetrafluoroborate (98%, Fluka), Na_2S nanohydrate (98%, Aldrich), ammonium thiocyanate (97.5%, Aldrich), sodium stannate trihydrate (95%, Sigma-Aldrich), C_6D_6 (99.9%, CIL), and DMSO-d_6 (99.9%, CIL) were used as received.

Synthesis of CdSe NCs. CdSe NCs were synthesized following the established procedure.[25] For preparing the cadmium myristate precursor, cadmium nitrate solution in MeOH (5 mmol/50 mL) was added dropwise into Na myristate solution (obtained by dissolving 15 mmol NaOH and 15 mmol myristic acid in 500 mL of methanol). The resulting white precipitate was washed with methanol three times, and then dried at 70 °C. In a typical synthesis of CdSe NCs, cadmium myristate (1.132 g) and SeO_2 (0.222 g) were mixed with dried ODE (128 mL) in a 500 mL three-neck flask and heated to 240 °C at a rate of 20 °C/min (the solution has dried for 30 min at 100 C). After 3 min at 240 °C, 2 mL of dried oleic acid was injected, and the solution was cooled to ca. 140 °C, followed by the removal of ODE via vacuum distillation. After 30 min, when ca. 20 mL of ODE was left in the flask, the solution was cooled down to RT and CdSe NCs were washed 3 times with hexane and ethanol. After this purification step, CdSe NCs were redispersed in hexane and used for further experiments. For comparison, we also replaced Cd myristate by Cd oleate and obtained identical results in terms of particle size and chemical composition. The cadmium oleate precursor was prepared by mixing 0.250 g of CdO (2 mmol) and 6 mL of OA in 128 mL of ODE, heating to 240 °C until the mixture become colorless, followed by cooling to 100 °C, and drying under vacuum for 1 h.

Synthesis of Inorganic Ligands. SnS_2 was prepared according to ref 9a. $(N_2H_5)_4Sn_2S_6$ was obtained by dissolving elemental tin (118.7 mg, 1 mmol) in 3 mL of 1 M S/N_2H_4 solution and 1 mL of N_2H_4 upon stirring at ca. 100 °C for 3 days forming a slightly yellow solution. K_4SnS_4 was obtained by combining K_2S (0.22 g, 2 mmol) and SnS_2 (0.183 g 1 mmol) in 4 mL of water (stirring for 4 h at RT). Afterward, the solution was filtered, and white K_4SnS_4 was isolated by adding acetone (40 mL), followed by 3 rinses with acetone and vacuum-drying. All other chalcogenidometallates were isolated and dried in the same manner. $K_4Sn_2S_6$ was obtained in a similar manner to K_4SnS_4; however, the quantity of K_2S was adjusted (0.11 g, 1 mmmol). $K_6Sn_2S_7$ cannot be obtained in aqueous solution; however, it can be obtained in MFA by combining stoichiometric amounts of SnS_2 and K_2S or by dissolving K_4SnS_4 in MFA. K_3AsS_4 was prepared by combining As_2S_5 (0.310 g, 1 mmol) and K_2S (0.33 g, 3 mmol) and 10 mL of H_2O at room temperature. K_3SbS_4 was prepared by dissolution Sb_2S_3 (0.339 g, 1 mmol) in a solution containing K_2S (0.33 g, 3 mmol) and S (0.064 g, 2 mmol) in 10 mL of H_2O at RT. K_4GeS_4 was prepared by dissolving GeS (0.104 g, 1 mmol), in a solution containing K_2S (0.27g, 2.5 mmol), S (0.064 g, 2 mmol) in 10 mL of H_2O at 50 °C.

Organic-to-Inorganic Ligand Exchange. In a typical procedure, 50 mg of K_4SnS_4 (or $K_4Sn_2S_6$, K_2S, K_3AsS_4, K_3SbS_4, K_4GeS_4) was dissolved in 10 mL of FA or MFA and mixed with 10 mL of hexane solution of oleate-capped CdSe NCs (ca. 50 mg). The mixture was vigorously stirred for 30 min until the hexane phase became colorless and all NCs migrated into polar solvent. The hexane layer was carefully removed, and the polar phase was rinsed 3 times with pure hexane, and then filtered through a 0.2-μm filter. CdSe NCs were precipitated with a minimal amount of MeCN. For more efficient precipitation, MeCN can be mixed with a small amount of toluene (e.g., 10:1 ratio). For elemental analysis, NCs were redispersed in MFA and precipitated once again with MeCN. Analogous ligand exchange reactions were conducted with other solvents: H_2O (K_4SnS_4) and N_2H_4 (for the $(N_2H_5)_4Sn_2S_6$ ligand). In the case of N_2H_4, all steps were carried out in a glovebox. Ligand removal with Et_3OBF_4 was carried out according to known procedure,[13b] and stabilization with $(NH_4)SCN$ was performed according to the established procedure.[10d]

Nuclear Magnetic Resonance (NMR) Spectroscopy. Liquid state ^{119}Sn NMR spectra were recorded at 186.5 MHz using a Bruker 500 MHz DRX spectrometer. Spectra were obtained at room temperature without deuterium locking of the main magnetic field. The pulse width was set at 10 μs, and the relaxation delay was 0.5 s. The number of scans used for experiments was 4800. The NMR samples were prepared in 5 mm tube in glovebox/air using high purity solvents (C ∼ 0.05 M). All ^{119}Sn chemical shifts were referenced to $Sn(CH_3)_4$. The latter, sealed in a capillary, was also used as an internal standard for accurate normalization of all spectra enabling the quantification of the amounts of absorbed thoistannates. Liquid state ^1H NMR spectra were recorded using Bruker 250 and 300 MHz spectrometers. Spectra were obtained at room temperature with locking of the main magnetic field. The pulse width was set at 11.5 μs, and the relaxation delay was 2 s. The number of scans used for experiments was 32. The NMR samples were prepared in 5 mm tubes using C_6D_6 or DMSO-d_6 as solvents. All spectra were referenced to tetramethylsilane. Solid-state CPMG[26] (Car−Purcel−Meiboom−Gill; CPMG is a spin echo pulse sequence consisting of 90° radio frequency pulse followed by an echo train induced by successive 180° pulses) MAS ^{119}Sn spectra of dry powdered materials were acquired on a 700 MHz spectrometer ($\nu_0(^{119}Sn)$ = 261.06 MHz) with a 2.5 mm double resonance probe at reduced temperature (250 K). Sample spinning rates of 25 kHz were employed. For the crystalline materials ^{119}Sn NMR spectra could be acquired in reasonably short experiment times. However, the ^{119}Sn longitudinal relaxation times were very long as signal could only be observed with lengthy recycle delays (>60 s). CPMG spectra are shown in their echo reconstructed form. They were obtained by summing the whole echoes of the FIDs in the time domain, followed by Fourier transform and application of a first order phase correction.[26] ^{119}Sn chemical shifts were referenced to $Sn(CH_3)_4$.

X-ray Absorption Spectroscopy. This was carried out at the X10DA (Super XAS) beamline at the Swiss Light Source, Villigen, Switzerland, which operated with a ring current of approximately 400 mA in top-up mode. The polychromatic radiation from a superbend magnet, with a magnetic field of 2.9 T and critical energy of 11.9 keV, was monochromatized using a channel cut Si(311) crystal monochromator. Spectra were collected on pressed pellets optimized to 1 absorption length at the Sn K-edge (29 200.1 eV) in transmission mode. For absolute energy calibration, the absorption of a Sb foil was measured simultaneously between the second ionization chamber and third ionization chamber. All 30 cm long ionization chambers were filled with Ar. Spectra were normalized using Athena,[27] and EXAFS spectra were fitted using FEFF[28] interface Artemis.[27] Fourier transformation of the background-subtracted EXAFS spectra was carried out in a *k*-range from 3 to 12 $Å^{-1}$, with a δk of 1. Fitting of the EXAFS data was realized using scattering path obtained from theoretical standards for Na_4SnS_4, $Na_4Sn_2S_6$, $Na_6Sn_2S_7$. The Sn−S coordination shell was fitted first, in a range from 1 to 2.6 Å, without constraining the fitting parameters (amplitude reduced factor s_0^2, energy shift E_0, bond distances Δr, Debye−Waller factor σ^2). The amplitude reduction factors were calibrated first for the free ligands (coordination number fixed at 4). Then, for the second shell, CN, E_0, and Δr were fixed at their best value, and the fit range was extended to 4 Å in order to determine the parameters for the second shell. Cd atoms were introduced into the existing paths by replacing the Na atoms. The scattering path of the second shell Sn−Cd was added to the fits with its own set of s_0^2 and Δr. Fitting of both shells provided a single energy shift and Debye−Waller factor valid for both shells, as well as amplitude reduced factor and bond distances for each shell.

DOI: 10.1021/ja510862c
J. Am. Chem. Soc. 2015, 137, 1862−1874

Scheme 1. Schematics of the Organic-to-Inorganic Ligand Exchange on the Surface of CdSe NCs Showing the Formation of Fully Inorganic Composition (1) That Retains All Cd Atoms[a]

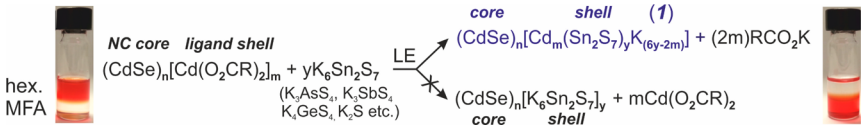

[a]The second possible pathway corresponds to loss of molecular Cd-oleate and was not observed in this study.

Inductively Coupled Plasma Optical Emission Spectrometry. (ICP-OES) was carried out using commercial ICP-OES spectrometer (Spectro Arcos, SPECTRO Analytical Instruments GmbH, Kleve, Germany). Experimental conditions for all measurements were the same and are summarized in Supporting Information Table S1. Every sample was measured 3 or 5 times, and the average result is reported. Samples were prepared by microwave-assisted digestion in a closed container of the dried materials in a mixture of 3 mL of HNO_3, 3 mL of HCl, and 0.5 mL of H_2O_2. Mn was used to control the digestion recovery. Element quantification was carried out by external calibration.

Other Characterization. UV−vis absorption spectra for colloidal solutions were collected using a Jasco V670 spectrometer in transmission mode. Attenuated total reflectance-Fourier-transform infrared spectra (ATR-FTIR, in mid-IR and far-IR spectral regions) were recorded using Thermo Scientific Nicolet 6700 FT-IR spectrometer. Powdered samples were deposited onto Si substrates, turned upside down, and pressed against the diamond ATR crystal. For quantifying the removal of initial organic ligands, FTIR spectra were calibrated with internal standard KCN added to the sample (CN stretches are well separated from CH). Liquid samples were measured by placing a small droplet directly onto ATR crystal. Raman spectra were recorded with a Renishaw inVia Raman microscope. Samples were run with a 785 nm laser, with 64 × 2 s scans at 2 mW power.

Calculation of the Ligand Surface Coverage. The wavelength of the $1S_e-2S_{h1/2}$ transition maximum was used to determine the mean NC diameter.[29] From the NC size, the number of CdSe units per crystals was calculated, assuming a spherical shape and the molar volume of bulk cadmium selenide. The concentration of the NCs, the ratio of ligands per nanocrystal, and the ligand surface density assuming spherical shape were calculated from the number of CdSe units per NCs, the molar concentration of CdSe, and ligands in solutions.

DFT Simulations. Calculations were carried out using the Quickstep module of the CP2K program suite.[30] CP2K is freely available from http://www.cp2k.org/ and utilizes a dual basis of localized Gaussians and plane waves.[31] The plane wave cutoff was 300 Ry, appropriate for the Goedecker−Teter−Hutter pseudopotentials[32] that we employed, and the localized basis set of double-ζ plus polarization (DZVP) quality optimized to reduce the basis set superposition errors.[33] Calculations were performed using the Perdew−Burke−Ernzerhof (PBE) exchange correlation functional. Simulations were performed with nonperiodic boundary conditions in a 50 × 50 × 50 $Å^3$ unit cell for 2.5 and 3 nm NC sizes. The NC core was carved out of bulk zinc blende CdSe. All single-bonded atoms were discarded, resulting in a faceted cuboctahedron shape. Cd-rich (100) facets with two dangling bonds per atom were passivated with ligands, whereas (111) facets with one dangling bond per atom were left intact and facet passivation was achieved by adding surface vacancies, as described previously.[24] Chlorine was used for simplicity as a ligand electronically similar to oleate, except for calculation of oleate binding energy where it was taken explicitly. Care was taken to select the stoichiometry that preserves the charge neutrality of the dot, necessary to position the Fermi level in the midgap.[34] In case of MCC adsorption, the ligand was added together with potassium counterions in the amount required to maintain the charge neutrality. All geometries were initially propagated through a molecular dynamics simulation of at least 1 ps and then relaxed until forces on atoms reduced below 40 meV/Å. Optimized geometries and full input files for simulations are provided in Supporting Information.

RESULTS AND DISCUSSION

Carboxylate−Metal Chalcogenide Complex Ligand Exchange. It is known that carboxylate ligands can be fully exchanged with MCC ligands,[9,23a] but details of this process are lacking. As shown by Owen et al.,[22f] carboxylate (oleate, myristate, etc.) can be removed as an anionic (X-type) RCO_2^- moiety or as a $Cd(O_2CR)_2$ molecule, depending upon the type of incoming ligand (anionic or neutral molecule). Furthermore, the atomic structure of inorganic MCC ligands in solution at the NC surface and their bonding motifs at the NC surface are poorly understood. We have chosen ∼3.5 nm carboxylate-terminated zinc blende (zb) CdSe NCs[25] as a model system for studying the LE reactions with MCC ligands. According to the detailed surface chemistry study by Owen and co-workers,[22f] the structure of carboxylate-capped CdSe NCs can be represented with the formula $(CdSe)_n[Cd(O_2CR)_2]_m$, where carboxylate surface coverage is 1.5−4 carboxylates/nm^2, depending upon the purification procedure and nature and quantity of solvents and surfactants used. Hence the overall NC stoichiometry is Cd-rich. No other ligands such as neutral molecules of phosphines or amines (L-type ligands) were involved in the preparation of such CdSe NCs, thus providing a well-defined and simple starting material for LE reactions. We began our study by addressing the initial key question about the actual mass-balance during the LE reaction with MCCs.

Fate of Oleate and the Mass Balance of the LE Reaction. The organic-to-inorganic LE was carried out via a phase-transfer reaction (Scheme 1). The initially carboxylate capped CdSe NCs migrate from the nonpolar phase (hexane) to a polar phase (MFA or N_2H_4) upon LE due to the change from a hydrophobic surface functionality (with steric stabilization) to a hydrophilic surface functionality (electrostatic stabilization). Note that this is the first time that several of these MCCs have been used as capping ligands ($K_6Sn_2S_7$, K_4GeS_4, K_3SbS_4). For comparison, LE reactions were also performed with a metal-free S^{2-} ligand and with Et_3OBF_4 (Meerwein's salt).[13b] To the best of our knowledge, MFA has the highest known static dielectric constant (ε = 176) for solvents; therefore, MFA enables the efficient dissociation of cations, leading to stable colloidal solutions. In order to remove any unbound ligands following LE, the NCs are precipitated from the MFA phase by adding a minimal amount of nonsolvent (usually MeCN). The nonsolvent and its quantity are chosen such that the free ligands remain soluble in the solvent/nonsolvent mixture. The LE reaction mass-balance was estimated by quantitative elemental analysis (ICP-OES, Supporting Information Tables S1 and S2), ATR-FTIR, and ^1H and ^{119}Sn NMR spectroscopies of all phases: initial oleate-capped NCs, precipitated thiostannate-capped NCs, and hexane and MFA phases collected after phase-separation,

DOI: 10.1021/ja510862c
J. Am. Chem. Soc. 2015, 137, 1862−1874

including all supernatants. For ICP-OES analysis, all dried residues were acid digested using standard procedures. Results are detailed below.

As expected from the formula $(CdSe)_n[Cd(O_2CR)_2]_m$, the initial oleate capped 3.5 nm spherical NCs are Cd-rich, and a Cd:Se atomic ratio of 1.22 was determined by ICP-OES analysis. In all cases ATR-FTIR, and NMR spectra indicate removal of at least 99.9% of the initial oleate ligands from the NC surface following LE (Supporting Information Figures S1 and S2). Figure 1 shows the optical absorption spectra of the

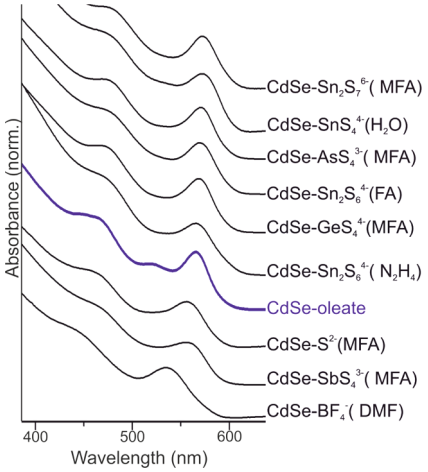

Figure 1. Absorption spectra of ~3.5 nm CdSe NCs capped with initial oleate ligands and, after ligand exchange, with various chalcogenidometallate complexes, sulfide ions, or weakly bound BF_4^- ions.

NCs capped with the initial oleate ligand and capped with various MCCs, sulfide ions, or weakly bound BF_4^- ions. The excitonic absorption peak of the MCC and sulfide capped CdSe NCs exhibit only small red shifts (1−11 nm) and a blue shift of ~11 nm, respectively, in comparison to the excitonic absorption peak of the initial oleate capped NCs. This suggests that there are only small differences in the radius of the particles following LE with these inorganic ligands. On the other hand, LE with Et_3OBF_4 leads to a noticeable ~25 nm blue shift of the excitonic absorption peak (Figure 1) and a Se-rich stoichiometry of the NCs (Supporting Information Table S2). This blue shift corresponds to decrease of NC diameter by ca. 0.5 nm (a Cd−Se bond is *ca.* 0.2−0.3 nm long, depending upon the crystallographic direction) or ca. 35% reduction in volume (from 22.4 to 14.2 nm^3). Presumably, Et_3OBF_4 removes not only the oleate capping ligands, but also an excessive monolayer of Cd atoms as a highly soluble $Cd(BF_4)_2$ salt. Another characteristic effect of LE is the disappearance of the second absorption peak ($2S_{h2/3}-1S_e$) in all inorganic capped NC samples. A similar effect has also been observed by Owen et al.[22f] and by others in studies dealing with LE reactions with organic ligands.[35] Nondiscrete separation between the $1S_{h2/3}$ and $2S_{h2/3}$ hole levels is most plausibly explained by heterogeneity of the surface hole states due to increased stoichiometric (e.g, incorporation of S) and structural surface irregularities.[36]

ICP-OES elemental analysis indicates that all MCC capped NCs retain a Cd-rich stoichiometry, with Cd:Se ratios of 1.15−1.30 (Supporting Information Table S2). Increased Cd stoichiometries may be caused by partial anion exchange of Se-to-S at the NC surface. ICP-OES analysis of the hexane phase following LE shows that less than 1% of Cd remained in the hexane phase. Upon precipitation and separation of NCs, less than 0.1% of Cd can be found in MFA. Consequently, no more than 5% of the Cd from the initial $Cd(O_2CR)_2$ ligand shell is detached from the NC surface during the LE reactions with MCCs and sulfide as ligands. Somewhat contrary to the common notion that long-chain organic ligands should remain in the nonpolar phase, ^1H solution NMR spectra indicate no residual oleate-anions in hexane phase after LE, but rather large amount of potassium oleate in the MFA phase following LE (Supporting Information Figure S3, vinylic hydrogens at δ = 5.1−6.1 ppm were monitored). Quantitatively, the amount of potassium oleate corresponds to ca. 2 carboxylates/nm^2 of the initial CdSe NCs, consistent with the density of 1.5−4 carboxylates/nm^2 reported by Owen et al.[22f] The amount of incoming MCC ligands varies from 0.65 to 2 MCC ligands/nm^2. Taken together, ICP-OES and ^1H NMR experiments on NCs and supernatant solutions provide strong evidence for the formation of the all-inorganic MCC-capped CdSe NCs with the composition expressed with formula 1 in Scheme 1. This implies the purely X-type ligand-exchange and the formation of Cd−S bonds at the NC/MCCs interface.

Solution Phase Behavior of Sn−S MCCs and Their Adsorption onto NC Surface. $Sn_2S_6^{4-}$ and SnS_4^{4-} anions were introduced by Krebs[37] and later studied by Kanatzidis,[38] Dehnen,[39] and others. These ions are very convenient for solution NMR studies due to good sensitivity of (natural abundance) ^{119}Sn NMR, with spin of $^1/_2$ leading to narrow NMR peaks. Thiostannate anions often interconvert depending upon the solvent or pH, while their isotropic chemical shifts ($\delta(^{119}Sn)$) are well-documented and rather weakly solvent or counterion dependent.[39a] $\delta(^{119}Sn)$ values of all thiostannate anions fall in relatively narrow range 49−74 ppm indicating that the tetrahedral environment for ^{119}Sn nuclei is maintained, whereas the change in coordination number by 1 would lead to ca. 150 ppm change in chemical shift. No SnS_3^{2-} anions were observed in our solution NMR studies.[40] No other Sn species, such as tin-oxosulfide ions, were detected by NMR spectroscopy (from −1000 to 1000 ppm). $SnTe_4^{4-}$ ions differ from thiostannate ions in that they contain more polarizable Te atoms, and therefore, their ^{119}Sn chemical shifts are highly variable due to solvation or ion-pairing effects and are generally observed between −1675 and −1825 ppm.[41] Furthermore, Se- and Te-based stannates are much more sensitive to oxygen. For these reasons, we concentrated our solution NMR studies exclusively on thiostannate ions.

Before studying the LE reaction with solution NMR spectroscopy, we studied the actual species existing in solutions of these thiostannate compounds in nonaqueous solvents commonly used in LE reactions. K_4SnS_4 and $K_4Sn_2S_6$ can be prepared in water by combining SnS_2 with the correct molar proportions of K_2S. Figure 2 shows the effect of the solvent, as observed by solution ^{119}Sn NMR, upon dissolution of the pure substances K_4SnS_4 and $K_4Sn_2S_6$. The most interesting observation is the appearance of highly charged $Sn_2S_7^{6-}$ ions as the predominant ion in MFA solutions upon dissolving K_4SnS_4. An analogous NMR spectrum is obtained by combining SnS_2 and K_2S directly in MFA. $Na_6Sn_2S_7$ has been previously obtained by solid-state synthesis by Krebs et al.[37a] and characterized with solid-state NMR spectra by Mundus et al.[42] A clear spectroscopic signature that distinguishes $Sn_2S_7^{6-}$ from $Sn_2S_6^{4-}$ is the presence (in good agreement with natural

DOI: 10.1021/ja510862c
J. Am. Chem. Soc. 2015, 137, 1862−1874

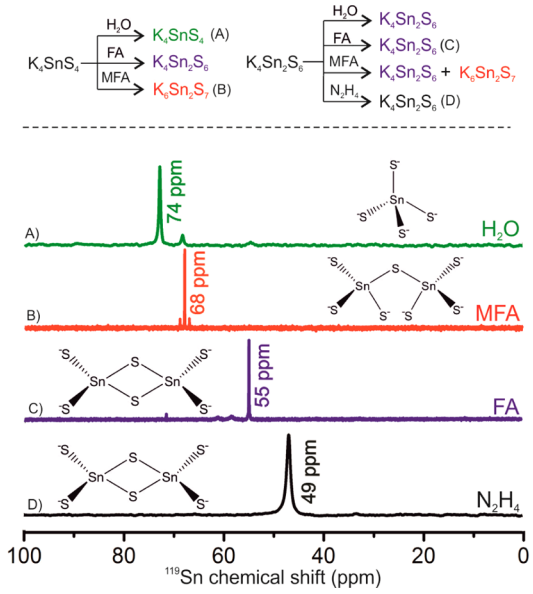

Figure 2. General scheme for transformations of K_4SnS_4 and $K_4Sn_2S_6$ upon dissolution in H_2O, FA, MFA, and N_2H_4. Solution ^{119}Sn NMR spectra of K_4SnS_4 dissolved in H_2O (A, 74 ppm), K_4SnS_4 dissolved in MFA (B, 68 ppm corresponding to $K_6Sn_2S_7$, see main text), $K_4Sn_2S_6$ in FA (C, 55 ppm, corresponding to $K_4Sn_2S_6$), $(N_2H_4)_4Sn_2S_6$ in hydrazine (49 ppm). Two kinds of S atoms are present in SnS_4^{4-} (4 terminal, 0 bridging), $Sn_2S_6^{4-}$ (4 terminal, 2 bridging), and $Sn_2S_7^{6-}$ (6 terminal, one bridging).

abundances of ^{117}Sn nuclei) of weaker satellite peaks caused by heteronuclear two bond $^{119}Sn-S-^{117}Sn$ spin–spin coupling. The $^2J(^{119}Sn, ^{117}Sn)$ coupling constant in $K_6Sn_2S_7$ is 349.4 Hz which is in good agreement with literature.[43] In the rigid $Sn_2S_6^{4-}$ this coupling seems to be absent or much weaker, possibly due to poorer S-orbital overlap caused by the rigid conformation of Sn_2S_2 ring.[40] A lack of coupling could also occur because of a dynamic process such as equilibria between two kinds of thiostannate ions or if the Sn–S bridging bonds are labile.

A clear distinction between all three thiostannate ions can be obtained also by Raman spectroscopy (Figure 3). The solid-state Raman spectrum of $K_4Sn_2S_6$ is characterized by two symmetric $Sn-S_{terminal}$ vibrations at 386 and 373 cm^{-1}, vibration of Sn_2S_2 ring at 277 cm^{-1}, and $Sn-S_{bridging}$ vibration at 347 cm^{-1};[18b,37d,44] K_4SnS_4 exhibits only two bands at 351 and 370 cm^{-1}, characteristic of symmetric and asymmetric Sn–S modes.[18b,37a] The spectrum of solid $K_6Sn_2S_7$ isolated from MFA is characterized by the strong band at ca. 360 cm^{-1}, presumably due to $SnS_3-S-SnS_3$ bridges, while the other two modes at 340^{-1} and 380 cm^{-1} are assigned to Sn–S vibrations (similar to SnS_4^{4-}). The solution phase Raman spectra of $Sn_2S_6^{4-}$ in FA and $Sn_2S_7^{6-}$ in MFA resemble those of the solid-state samples. Further illustrating the effect of solvent, the pH value of the solution plays an important role as well. $Sn_2S_7^{6-}$/MFA converts into $Sn_2S_6^{4-}$/MFA upon addition of KOH K_2S (that reacts with residual moisture giving KOH and KHS). This can be explained by the importance of protonation for the stability of $Sn_2S_7^{6-}$. In N_2H_4, only $Sn_2S_6^{4-}$ is stable, and it does not convert into SnS_4^{4-} or $Sn_2S_7^{6-}$ upon addition of S^{2-} (Supporting Information Figure S4). On the basis of the above solution ^{119}Sn NMR and Raman spectroscopic data, we further studied the LE with the oleate capped NCs for four ligand/solvent combinations. Only those ligand/solvent

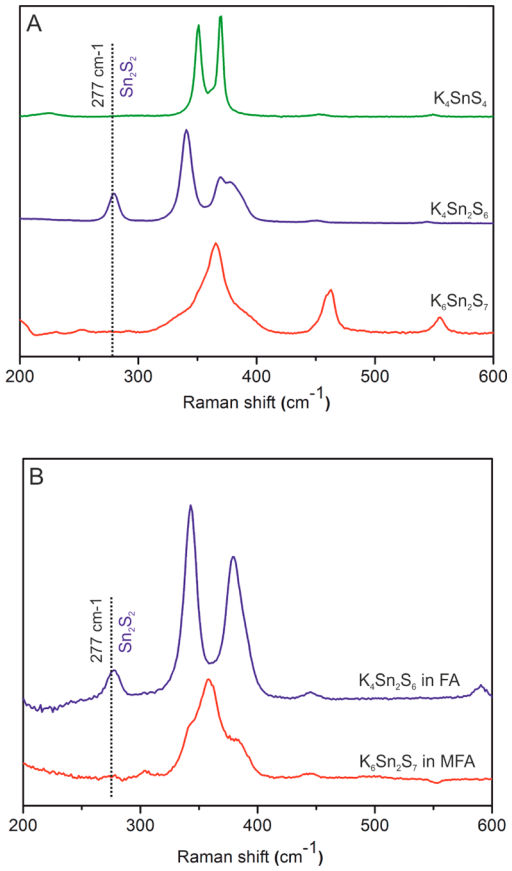

Figure 3. (A) Raman spectra of solid K_4SnS_4 (green), $K_4Sn_2S_6$ (blue), and $K_6Sn_2S_7$ (red). (B) Solution-phase Raman spectra of $K_4Sn_2S_6$ in FA (blue) and $K_6Sn_2S_7$ in MFA (red).

combinations which clearly yield a single form of anion without altering the pH of the solution (Figure 2) were chosen: SnS_4^{4-}/H_2O, $Sn_2S_6^{4-}$/FA, $Sn_2S_6^{4-}$/N_2H_4, and $Sn_2S_7^{6-}$/MFA.

Upon binding of the anions to the NC the isotropic molecular tumbling slows, leading to significant broadening and attenuation of NMR signals from bound ligands.[45] The NMR signal broadening arises from large anisotropic dipolar couplings and anisotropies of the chemical shifts which are no longer averaged away.[46] In the case of MCC ligands bound to the NC surface, the signal mostly vanishes (Figure 4), allowing quantitative estimation of the amount of surface-bound ligands by measuring intensity from the remaining unbound ligand. Thiostannate ligands can act as polydentate ligands due to multiple terminal S atoms. On the basis of the LE reaction shown in Scheme 1, the following solution equilibrium between bound and unbound MCC ligand can be postulated assuming $K_6Sn_2S_7$ as a single thiostannate form in MFA:

$$(CdSe)_n[Cd_m(Sn_2S_7)_y\overset{(\mathbf{1a})}{K_{(6y-2m)}}] \rightleftarrows (CdSe)_n[\overset{(\mathbf{1b})}{Cd_m}(Sn_2S_7)_{m/3}]+(y-m/3)K_6Sn_2S_7 \quad (1)$$

The exchange of bound and unbound MCC ligand is rather slow, as the NMR spectra for unbound ligands do not show broadening or a change in the chemical shift which would indicate fast exchange of bound and unbound ligand.[22g] Composition **1b** represents an extreme case, in which full denticity of $Sn_2S_7^{6-}$ is used (κ^6-$Sn_2S_7^{6-}$ in the terminology of

DOI: 10.1021/ja510862c
J. Am. Chem. Soc. 2015, 137, 1862–1874

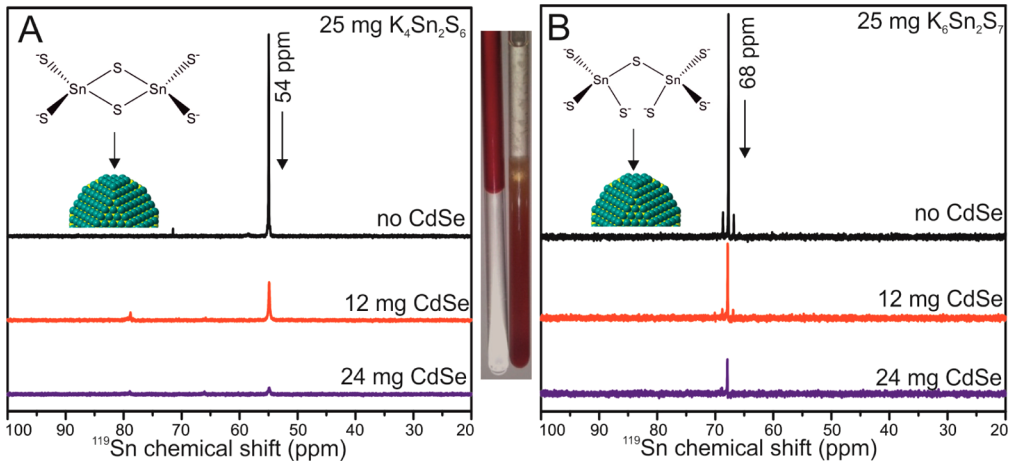

Figure 4. Solution ^{119}Sn NMR spectra for $K_4Sn_2S_6$/FA and $K_6Sn_2S_7$/MFA solutions before LE, and after LE with increasing amounts of CdSe NCs. Note that 24 mg of CdSe NCs corresponds to y/m ratio of ca. 2−2.2 in eq 1; i.e., the amount of thiostannate ligand is sufficiently high for monodentate binding to all surface Cd atoms. Inset shows NMR tubes before and after LE.

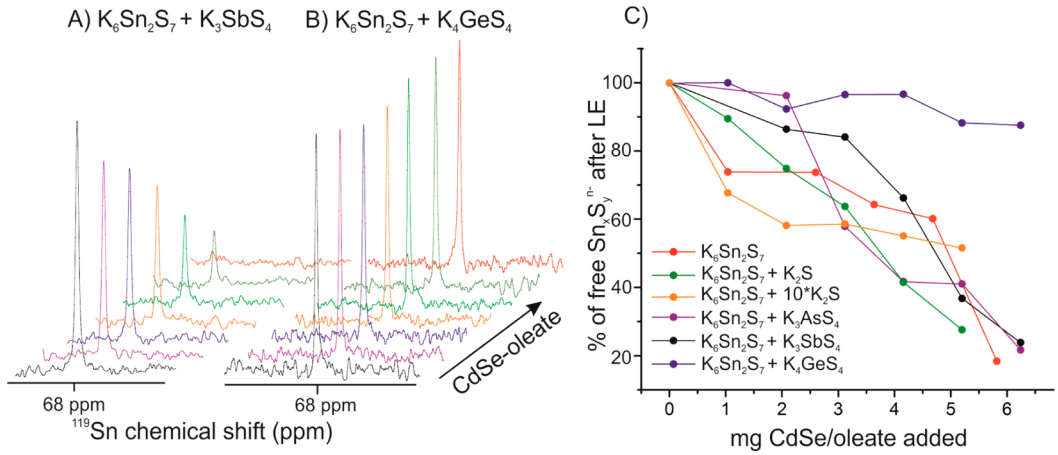

Figure 5. Concurrent LE reaction by adding oleate-capped CdSe NCs into solutions of (A) $K_6Sn_2S_7$ and K_3SbS_4 or (B) $K_6Sn_2S_7$ and K_4GeS_4. (C) A graph illustrating the decrease of the integrals of the ^{119}Sn NMR signal upon titration with oleate-capped CdSe NCs (6 mg = 32 μmol). The initial $K_6Sn_2S_7$ was 5 mg (7 μmol) in a 0.5 mL reaction volume. All ligand mixtures are equimolar, except where 10-fold access is indicated.

coordination chemistry); that is, each $Sn_2S_7^{6-}$ forms 6 bonds with surface Cd^{2+}. An opposite extreme is the κ^1-$Sn_2S_7^{6-}$ bonding motif, that is, monodenticity of the ligand at $y = 2m$. Thus, in principle the amount of surface-bound $Sn_2S_7^{6-}$ ligand can adopt values of $m/3 \leq y \leq 2m$, due to facile rearrangement of Cd-MCC bonds with variable denticity of MCC ligand. Quantitatively, after first addition of oleate-capped CdSe NCs (12 mg, Figure 3B), the $K_6Sn_2S_7$ ligand coverage was ∼4 ligands nm^{-2}. Note that this coverage corresponds to $y \approx 2.5m$, which exceeds the $2m$ limit discussed above, but may be explained by the additional week nonspecific binding of MCCs. After the number of CdSe particles in solution was doubled, the amount of ligands on the surface decreased to 2.2 ligands nm^{-2} for $K_6Sn_2S_7$, which corresponds to $y \approx 1.4m$. This shows that the initial binding of $K_6Sn_2S_7$ is labile and $K_6Sn_2S_7$ can detach and engage in a LE reaction with the oleate-capped CdSe, in agreement with postulated equilibrium reaction 1. After double precipitation with MeCN, the ICP-OES analysis shows 1.2 L nm^{-2}, that is $y \approx 0.7m$. Note that single-washed NCs are still well-dispersible in MFA, whereas double-washed NCs show much lower solubility in MFA, the difference which is best seen for larger NCs. When y approaches $m/3$ (composition **1b**) due to further washing steps, particles should contain no K^+ rendering them fully insoluble in polar solvents. Fully analogous observations are found for $K_4Sn_2S_6$ and other MCC ligands.

It is also important to note that the reverse exchange, e.g., displacement of MCCs by K-oleate and transfer of CdSe NCs back to the nonpolar phase, requires 20-fold molar excess of oleate, and takes up to 1−2 weeks, compared to minutes for direct LE. This is again in agreement with strong multidentate binding of thoistannate ligands to the NCs surface.

Concurrent MCC LE Reactions. Convenient monitoring of thiostannate concentrations by ^{119}Sn solution NMR also allows qualitative comparison of concurrent LE reactions with other MCC ligands. For example, when a 1:1 molar mixture of $K_6Sn_2S_7$ and K_3SbS_4 (Figure 5) or $K_6Sn_2S_7$ and K_3AsS_4 (Supporting Information Figure S5) is reacted with oleate-capped CdSe NCs the solution ^{119}Sn NMR signal in NMR spectra decreases at the same rate as for pure $K_6Sn_2S_7$, pointing to preferential binding of $Sn_2S_7^{6-}$ ions as compared to the other MCC. However, a $K_6Sn_2S_7$:K_4GeS_4 mixture shows no signs of $K_6Sn_2S_7$ binding to the NC surface during the phase transfer of CdSe NCs, suggesting that GeS_4^{4-} has a stronger binding affinity. The comparison of metal-free S^{2-} with MCCs is another important point, especially because S^{2-} is expected in

DOI: 10.1021/ja510862c
J. Am. Chem. Soc. 2015, 137, 1862−1874

the solutions of most MCCs. Only when a 10-fold excess of K_2S with respect to $K_6Sn_2S_7$ is added do we notice a slower decrease in the Sn signal in comparison with pure $K_6Sn_2S_7$-based LE (Figure 5C). Hence a binding affinity sequence $K_4GeS_4 > K_6Sn_2S_7 > K_3SbS_4$ (K_3AsS_4) $> K_2S$ can be established for the organic-to-inorganic LE.

Solid-State ^{119}Sn NMR Observation of Thiostannate Ligands Bound to the NC Surface. Having confirmed that thiostannate ions disappear from the solution and bind to the NC surface as a result of the LE reaction, we now turn our focus on the establishing bonding motifs at the NC/MCC surface. We used solid-state magic angle spinning (MAS) ^{119}Sn NMR spectroscopy to average the anisotropic NMR interactions and obtain solution-like NMR spectra of the MCC capped NCs.[40,47] The ^{119}Sn solid-state NMR spectra of the MCC capped NCs are compared to spectra of the pure solid unbound ligands and with the solution ^{119}Sn NMR chemical shifts of the dissolved ligands (Figure 6).

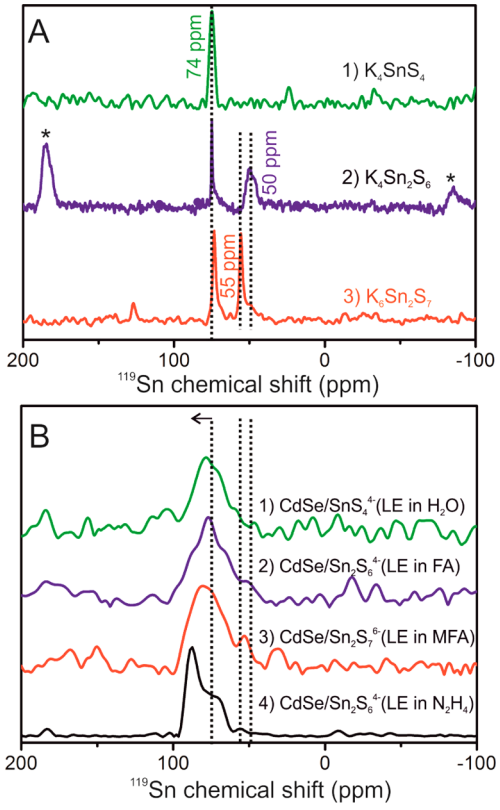

Figure 6. (A) Solid-state MAS ^{119}Sn NMR for K_4SnS_4, $K_4Sn_2S_6$, and $K_6Sn_2S_7$ powders. (B) Solid-state CPMG MAS ^{119}Sn NMR for CdSe/K_4SnS_4 (LE in H_2O), CdSe/$K_4Sn_2S_6$ (LE in FA), CdSe/$K_6Sn_2S_7$ (LE in MFA), and CdSe/$K_4Sn_2S_6$ (LE in N_2H_4). Three dash lines correspond to 74, 55, and 50 ppm, respectively (expected peaks for unbound ligands). The * represents the spinning side bands.

Similar to solution NMR spectra, $\delta(^{119}Sn)$ in the MAS ^{119}Sn NMR spectra of solid free ligands falls in the range 50−74 ppm. While the spectrum of solid K_4SnS_4 is characterized by one narrow peak at 74 ppm (in good agreement with the corresponding chemical shift for K_4SnS_4 dissolved in water), the spectrum of $K_4Sn_2S_6$ contains two peaks: one broad peak corresponds to $K_4Sn_2S_6$ at 50 ppm[42] and the narrow peak at 74 ppm from K_4SnS_4. The intensity of the isotropic K_4SnS_4 peak at 74 ppm appears to be more intense because the peaks from $K_4Sn_2S_6$ are much broader and also dispersed over several spinning side bands. Keeping in mind that the longitudinal relaxation rate of the $K_4Sn_2S_6$ peak also appeared to be slower, the NMR spectra indicate that at most only 10% of the $K_4Sn_2S_6$ sample corresponds to K_4SnS_4. The product isolated from $K_6Sn_2S_7$/MFA solution by adding acetonitrile shows signals at 74 ppm (50% integrated intensity, K_4SnS_4) and at 55 ppm (50%, attributed to $K_6Sn_2S_7$).

In order to overcome the low concentration of Sn atoms in the MCC capped NC samples, we applied a CPMG pulse sequence[26,48] to maximize the signal-to-noise of the spectra of the NC-ligand samples (Figure 6B). Overall, the chemical shifts fall in the same range as for the free ligands, indicating very similar tetrahedral SnS_4 environment of Sn. However, the peaks are considerably broader than those observed for the pure ligand samples, which is suggestive of a spread of binding motifs: various denticity conformations of ligands and distribution of binding sites on the NC surface (different facets, edges of facets, etc.). The downfield shifts of several ppm may arise due to binding of the thiostannate ions with the NC surface and from the formation of covalent Cd−S bonds. No unambiguous differentiation between SnS_4^{4-}, $Sn_2S_7^{6-}$, or $Sn_2S_6^{4-}$ can be made due to signal broadening. Furthermore, formation of SnS_2 on the NC surface can also be excluded, as it should manifest itself by the peak at −765 ppm in the solid-state ^{119}Sn NMR spectrum (for pure spectra of pure SnS_2 see Supporting Information Figure S6). No other Sn-containing species could be detected with solid-state NMR spectroscopy. In the case of CdSe/$K_4Sn_2S_6$/N_2H_4 samples, a clear splitting of ^{119}Sn NMR spectrum is observed that may indicate, for instance, two distinct binding modes of a ligand or mixed $Sn_2S_6^{4-}$/$Sn_2S_7^{6-}$ surface coverage.

^{77}Se CPMG MAS NMR spectra of CdSe NCs capped with thiostannate ligands contain a main peak at −528.5 ppm with ∼50 ppm broadening and a shoulder at −557.4 ppm (Supporting Information Figure S7). This line shape and more negative chemical shifts as compared to bulk CdSe (−472.3 ppm) are fully consistent with quantum-size effects and core−shell distribution of chemical shifts (more negative for near surface Se layer).[49]

Observation of Thiostannate Ligands on the NC Surface with Far-IR Spectroscopy. Far-IR spectroscopy (100−600 cm^{-1}) may serve as excellent tool for studying inorganic capping of colloidal NCs because this region corresponds to vibrational frequencies of bonds formed by heavier atoms such as Cd, Sn, and chalcogens and because organic ligands and other light-atom residues (solvents, etc.) show virtually no absorption. Previously, far-IR spectra were seldom used for characterization of colloidal NCs.[50] We note that, as expected, Raman spectra were not conclusive due to the fluorescence background from NCs and due to drastic difference in scattering intensity not only between solid NC cores (very weak signals) and molecular species (much greater signals), but between various molecules. Far-IR spectra of CdSe/oleate and "ligand-free" CdSe NCs (Figure 7) are very similar and contain a relatively narrow peak at 183 cm^{-1} characteristic of ν(Cd−Se) stretching frequencies,[51] and consistent with Raman shifts of transverse optical (156 cm^{-1}) and longitudinal optical (215 cm^{-1}) phonons.[52] The spectrum of CdSe/BF_4^- shows only peaks associated with CdSe. This is consistent with only weak electrostatic interactions between BF_4^- and the surface Cd^{2+} adatoms.

DOI: 10.1021/ja510862c
J. Am. Chem. Soc. 2015, 137, 1862−1874

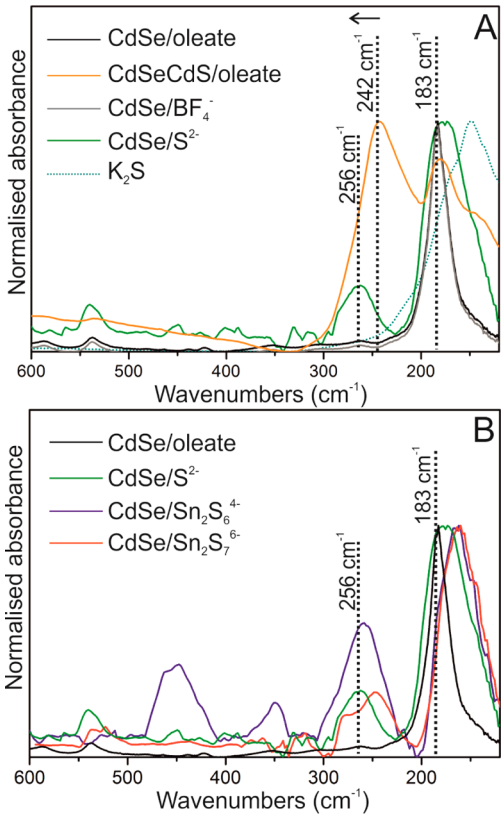

Figure 7. Far-IR ATR spectra for CdSe NCs with various surface chemistries. (A) CdSe/oleate (black), CdSeCdS/oleate (orange), $CdSe/BF_4^-$ (gray), $CdSe/S^{2-}$ (green), K_2S (dashed green spectrum). (B) CdSe/oleate (black), $CdSe/S^{2-}$ (green), $CdSe/Sn_2S_6^{4-}$ (blue), $CdSe/Sn_2S_7^{6-}$ (red).

Core–shell CdSe/CdS NCs (oleate capped, 4.5 nm core and 2 nm shell)[53] were also measured as a reference material for all MCCs in order to observe the effect of Cd–S bonds on the far-IR spectra. In CdSe/CdS NCs, a broad and intense peak at 242 cm^{-1} characteristic of CdS shell[51] and considerable broadening in CdSe region (with a small shoulder at 142 cm^{-1}, presumably due to the effects of strain and alloying at CdSe/CdS interface) were observed. In $CdSe/S^{2-}$ NCs, a broad shoulder at 260 cm^{-1} due to $Cd–S^-$ bonds[54] was slightly upshifted compared to pure CdS due to the formation of shorter Cd–S bonds at the NC surface than in pure CdS. Broadening of CdSe features was also observed. Figure 7B compares the far-IR spectra of CdSe NCs capped with different thiostannate ligands. The major common feature is intense absorption in the 240–300 cm^{-1} range due to the formation of Cd–S bonds. The broadening and downshift of CdSe band for $CdSe/Sn_2S_6^{4-}$ and $CdSe/Sn_2S_7^{6-}$ are very similar to $CdSe/S^{2-}$ and may also be the effect of the higher absorbance of ligands below 200 cm^{-1} (Supporting Information Figure S8). As expected, far-IR spectra of the pure K_4SnS_4, $K_4Sn_2S_6$, and $K_4Sn_2S_7$ compounds are distinctly different from each other, and from the surface-bound species, and agree well with the literature (see Supporting Information for further discussion).

Thiostannate Bonding Motifs from X-ray Absorption Spectroscopy and DFT Simulations. Qualitatively, both far-IR and NMR spectroscopy clearly indicate that thiostannate ions are covalently attached to the surface of CdSe, and on the basis of the NMR spectra, the basic four-coordinate SnS_4 coordination environment is preserved in all cases. Further insights into the binding modes and bond distances were gained with X-ray absorption spectroscopy (XAS). Sn K-edge XAS spectra allow the study of the local electronic and geometric structure (up to 6 Å) around Sn atoms, and are also applicable to disordered systems such as surface-bound ligands. In order to evaluate the data from the XAS measurements we took a Fourier transform of the spectra into frequency space, which results in a radial structure function (RSF) where peaks correspond to the distances to the nearest-neighbors. Fitting of the EXAFS region was performed using theoretical Sn–S references generated from crystal structures of Na_4SnS_4, $Na_4Sn_2S_6$, and $Na_6Sn_2S_7$. The value of the amplitude reduced factor (S_0^2) was determined by fitting the first shell using the references (S_0^2 = 4.6) and the coordination number (CN), Debye–Waller factor (DW), interatomic distance (R), and edge-shift (ΔE_0). For the free ligands, two major peaks could be distinguished in the RSFs (Figure 8A–C, Table 1), and they indicate close to expected interatomic distances (d) and coordination numbers (CN): only one type of Sn–S bond with d(Sn–S) = 2.4 Å and CN = 4 in K_4SnS_4, and two bonds in $K_4Sn_2S_6$ and $K_4Sn_2S_7$ [$Sn–S_1$ (terminal, ~2.35 Å) and $Sn–S_2$ (bridging, ~2.50 Å)] with CN close to the expected value (CN = 1–2). The bond lengths are in good agreement with crystallographic data[37] and with our DFT calculations.

Chemical binding of thiostannates to surface Cd atoms should modify the overall geometry of the ligand and its local coordination environment. Further, the surface conformation of a ligand will depend on the surface coverage, facet to which ligand binds, etc. It is therefore not possible to deduce the exact surface geometry, but rather to monitor the key differences to unbound ligands, primarily in the bond distances and coordination numbers. XAS studies on NCs after LE (Figure 8D–G) indicate important changes with respect to free crystalline ligands and unambiguously confirm chemical binding of thiostannate ligands onto NC surface. One important feature that was not directly observed by other techniques and reported here for the first time is that there is strong evidence for Sn–O bonds in XAS spectra of CdSe NCs capped with K_4SnS_4 in H_2O (d(Sn–O) = 2.1 Å). Judging from CNs, a particularly high proportion of Sn–O bonds are found in K_4SnS_4/H_2O (CN = 2.8 for Sn–O bonding) system, and only one type of Sn–S with d = 2.4 Å and CN = 1.3, suggesting an overall stoichiometry of $[SnO_3S]^{4-}$ (which can also correspond to a mixture of SnS_4^{4-} and SnO_4^{4-} ions). This can be explained by well-known hydrolysis of chalcogenidometallates in water at high pH, and this may also occur in nonaqueous solutions handled in air (as in this study). Also, CdSe NCs can aid the formation of Sn–O bonds in aqueous environment and even in powdered solids through photocatalytic oxidation of Sn–S by photogenerated holes. On the contrary, for the nonaqueous LE systems we observed a much smaller proportion of Sn–O bonds (CN = 0.2–0.9, Table 1). Further, and very importantly, two types of Sn–S bonds are found for $Sn_2S_6^{4-}$ and $Sn_2S_7^{6-}$, and all Sn–S distances are shorter, on average by 0.1 Å as compared to reference to unbound ligands, in agreement with DFT calculations (see below). The second coordination shell was fitted by introducing Cd (or Sn) atoms into the existing scattering paths by replacing the Na atoms and optimizing the parameters (Figure 8D,F,E,G). The shortest Sn–Cd distance of 3.37–3.8 Å was found for $Sn_2S_7^{6-}$ (CN ~ 1) and is attributed to Cd–S–Sn bridge which is in good agreement with the distances obtained by DFT modeling. We note that for NC-ligand

DOI: 10.1021/ja510862c
J. Am. Chem. Soc. 2015, 137, 1862–1874

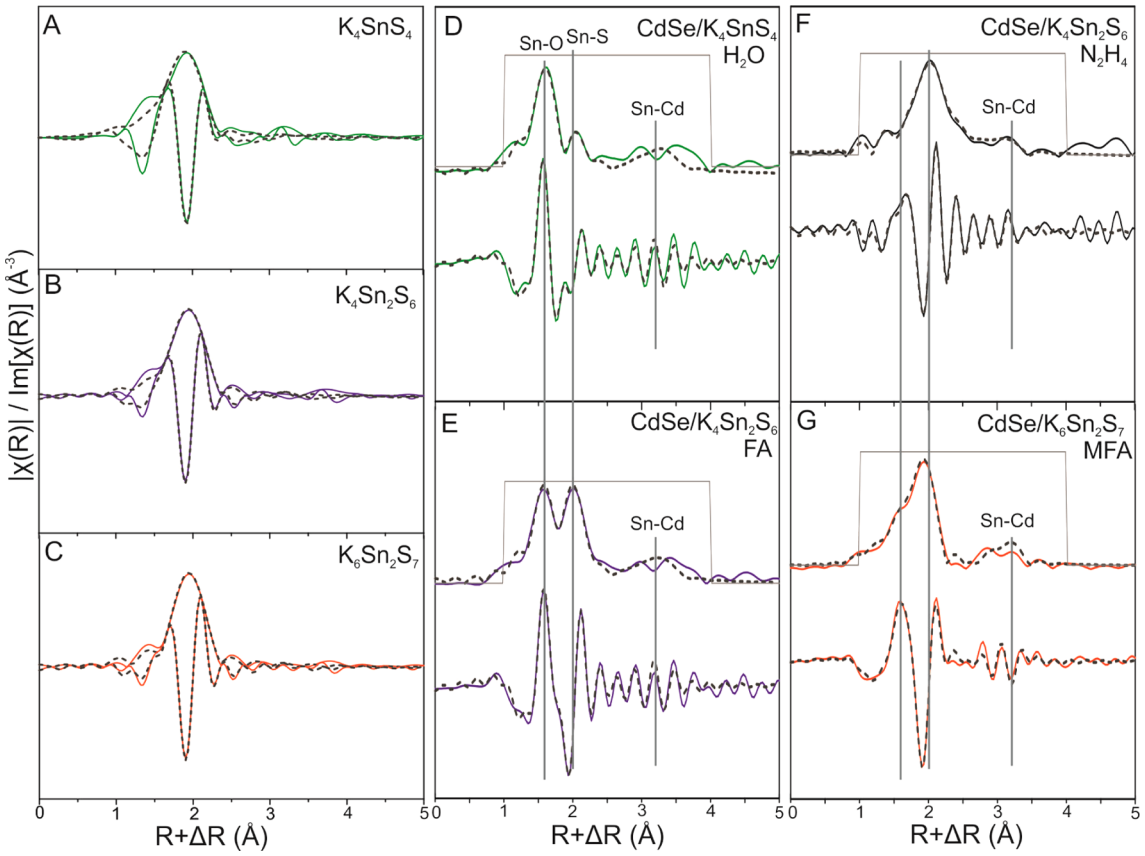

Figure 8. Fourier transform magnitude and imaginary part of the full XAS spectra of (A)K_4SnS_4, (B) $K_4Sn_2S_6$, (C) $K_6Sn_2S_7$ and (D) $CdSe/K_4SnS_4$ (LE in H_2O), (E) $CdSe/K_4Sn_2S_6$ (LE in FA), (F) $CdSe/K_4Sn_2S_6$ (LE in N_2H_4), (G) $CdSe/K_6Sn_2S_7$ (LE in MFA). Solid lines represent the experimental data; dotted lines represent the best fit. $R + \Delta R$ scale represents distances with phase correction.

Table 1. Structural Information for Reference Samples and Capped NCs from Best Fitting of the EXAFS Spectra (Figure 8)[a]

sample	path	CN	R_t (Å)	R_t DFT (Å)	DW (Å^2)	E_0 (eV)	*R*-factor
(free) K_4SnS_4	Sn−S	4.1 ± 0.6	2.41 ± 0.017	2.4	0.0107 ± 0.0025	2.03 ± 1.74	0.0075
(free) $K_4Sn_2S_6$	$Sn-S_{dangl}$	1.8 ± 0.4	2.34 ± 0.018	2.35	0.0010 ± 0.0019	6.68 ± 1.37	0.0043
	$Sn-S_{bridge}$	2.0 ± 0.5	2.46 ± 0.018	2.46			
(free) $K_6Sn_2S_7$	$Sn-S_{dangl}$	2.4 ± 0.9	2.37 ± 0.003	2.37	0.0008 ± 0.0009	8.17 ± 1.17	0.0078
	$Sn-S_{bridge}$	1.6 ± 0.8	2.48 ± 0.003	2.47			
$CdSe/Sn_2S_6^{4-}$/FA	$Sn-S_{dangl}$	1.4 ± 0.2	2.27 ± 0.016		0.0004 ± 0.0015	0.83 ± 0.29	0.0051
	$Sn-S_{bridge,surf}$	2.6 ± 0.7	2.42 ± 0.012		0.0004 ± 0.0015		
	Sn−O	0.7 ± 0.2	2.00 ± 0.019		0.0004 ± 0.0015		
	Sn−Cd	0.6 ± 0.2	3.77 ± 0.020		0.0024 ± 0.0010		
$CdSe/Sn_2S_7^{6-}$/MFA	$Sn-S_{dangl}$	0.7 ± 0.4	2.24 ± 0.057	2.27	0.0038 ± 0.0018	3.59 ± 0.88	0.0089
	$Sn-S_{bridge,surf}$	3.8 ± 0.7	2.41 ± 0.012	2.44	0.0038 ± 0.0018		
	Sn−Cd	0.9 ± 0.2	3.37 ± 0.012	3.99	0.0024 ± 0.0010		
$CdSe/Sn_2S_6^{4-}/N_2H_4$	$Sn-S_{dangl}$	1.1 ± 0.1	2.30 ± 0.009	2.25	0.0002 ± 0.0003	4.14 ± 0.91	0.0078
	$Sn-S_{bridge,surf}$	1.7 ± 0.2	2.44 ± 0.007	2.48	0.0002 ± 0.0003		
	Sn−O	0.2 ± 0.1	1.97 ± 0.033		0.0002 ± 0.0003		
	Sn−Cd	1.0 ± 0.7	3.51 ± 0.021	3.5−4.1	0.0063 ± 0.0063		
$CdSe/SnS_4^{4-}/H_2O$	Sn−S	1.3 ± 0.3	2.42 ± 0.020	2.31−2.44	0.0037 ± 0.0013	7.64 ± 0.93	0.0076
	Sn−O	2.8 ± 0.2	2.06 ± 0.011		0.0037 ± 0.0013		
	Sn−Cd	0.5 ± 0.2	3.51 ± 0.015	3.86	0.0002 ± 0.0001		

[a]Coordination number (CN), bond distance from XAFS (R_t), bond distance from DFT (R_t DFT), pseudo-Debye−Waller factor (DW), energy shift (E_0), *R* factor obtained from the fits.

samples the distances in the second shell are precisely fitted, while CN values are much less accurate.

For DFT simulations, theoretical models were prepared on the basis of the experimental findings: one terminal S atom from thiostannate ligand was coordinated to one adsorption site on the surface, displacing the original oleate (or halide) ligand, while each unbound terminal S was compensated by a potassium counterion. Calculations show that the thiostannate binding energy is 0.6 eV per site higher than for oleate, suggesting an energetically favored displacement. For a 3 nm

DOI: 10.1021/ja510862c
J. Am. Chem. Soc. 2015, 137, 1862−1874

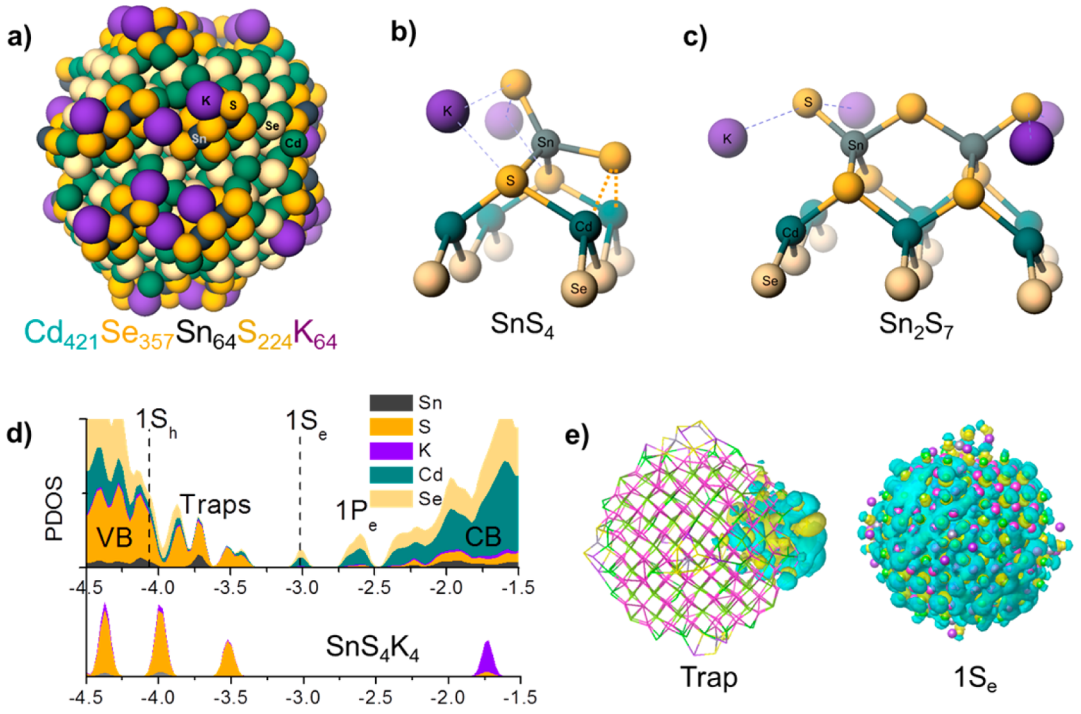

Figure 9. DFT modeling of thiostannate-capped CdSe NCs: (a) relaxed gometry of a 3 nm CdSe NC capped with $Sn_2S_7^{6-}$ ligands; (b) stable binding geometries of SnS_4^{4-} and $Sn_2S_7^{6-}$ ligands on (100) CdSe surface; (d) projected density of states for a free K_4SnS_4 ligand and for CdSe-K_4SnS_4 NC; (e) spatial distribution of the trap and electronic states in a 2.5 nm model.

model NC with exclusively $K_4Sn_2S_7$ capping ligand, such a procedure leads to a stable configuration with no S^{2-} or K_2S desorption, as verified by molecular dynamics. Calculated energy required for desorption of K_2S is 4.1 eV with explicit inclusion of coordinating MFA molecules. The relaxed structure with stoichiometry $Cd_{1.18}Se_1Sn_{0.18}S_{0.63}K_{0.18}$ is shown in Figure 9a. A similarly stable configuration can be constructed with K_4SnS_4.

To study the binding geometries in details, a smaller trap-free 2.5 nm CdSe model NC with one thiostannate ligand per facet was used. The (100) facets provide a tetrahedral lattice scaffold, helping maintain the tetrahedral coordination of Sn. For a SnS_4 complex it means two S atoms bind to the surface with the other two S unbound (Figure 9b). However, such dangling S atoms are highly unfavorable, and after relaxation one of them falls onto the surface by tilting the SnS_4 tetrahedron, and forming a bond to Cd (dotted lines) that breaks the periodicity of the original lattice. The remaining S is unable to distort the SnS_4 tetrahedron sufficiently in order to reach the surface and thus stays unbound, stabilized by the available potassium counterion. In the absence of potassium ions, this S atom tends to diffuse along the surface away from the SnS complex, exposing the Sn atom, or dimerizes with other available S from the same thiostannate complex or from complexes adsorbed nearby, thus stabilizing it against desorption. Similar behavior is observed for $Sn_2S_7^{6-}$ in which the bridging S makes the unit more rigid so that both dangling S cannot reach the surface (Figure 9c). For $Sn_2S_6^{4-}$, the rigid Sn_2S_2 ring precludes compliance with the underlying lattice; however, the ligand still maximizes its denticity by distorting the SnS_4 tetrahedra (see geometries in Supporting Information). Over the duration of our molecular dynamics runs we have not observed the fragmentation of $Sn_2S_6^{4-}$; however, we expect it to be quite possible. Overall, thiostannate complexes tend to maximize the amount of bonds to the surface, while counterions are found to be important for stabilization of Sn tetrahedral coordination. However, it is not uncommon for this tetrahedron to break.

Calculated distances in the relaxed geometries are presented in Table 1 and in general agree with EXAFS observations: the bond from Sn to dangling S is shorter, while Sn to surface-bound S and bridging S are practically identical and longer. EXAFS findings of slightly lower coordination numbers to dangling S may be indicative of rare detachment of a dangling S from Sn tetrahedra, as observed in theoretical model, but most of them remain intact. The theoretical model provides an Sn and Cd coordination numbers of 4, drastically different from EXAFS values. This can be attributed to inaccurate fitting of the second shell in EXAFS spectra of surface bound ligands. The predicted Sn−Cd distance of 3.86−3.99 Å is comparable to and slightly higher than experimental values.

The quality of surface passivation by thiostannate ions can be judged from the analysis of projected densities of states and HOMO and LUMO wave functions (Figure 9d,e). PDOS plots clearly show that thiostannate ligand creates hole traps on an initially trap-free NC which are localized mainly on dangling and bridging S atoms (Figure 9e). This is expected since the free ligand has HOMO levels deep in the bandgap of CdSe (Figure 9d). This is consistent with the low photoluminescence quantum yield (PL QY) of the MCC-capped CdSe NCs (usually below 1%)[9b] and drastically shorter ON-state in single-particle blinking trajectories of MCC-capped CdSe/CdS NCs.[55] Surprisingly, despite all the disorder of the surface (Figure 9a), the conduction band remains clear of traps thanks to self-healing also observed previously on ligand-free CdSe NCs,[56] consistent with excellent n-type conductivity of the CdSe-MCC films.[9b,14a]

DOI: 10.1021/ja510862c
J. Am. Chem. Soc. 2015, 137, 1862−1874

CONCLUSIONS

In conclusion, we have conducted a detailed experimental and theoretical study of the inorganic surface functionalization of CdSe NCs by thiostannate and similar sulfur-based ligands. The combined analysis of solution ^{1}H NMR, solution and solid-state ^{119}Sn NMR, far-IR and XAS spectroscopies, and DFT modeling is consistent with the X-type ligand exchange mechanism. During the ligand exchange reaction, CdSe NCs retain their Cd-rich stoichiometry, where surface Cd adatoms serve as binding sites for terminal S atoms from chalcogenidometallate ligands leading to all-inorganic $(CdSe)_{core}[Cd_m(Sn_2S_7)_y\text{-}K_{(6y-2m)}]_{shell}$ stoichiometry, taking $Sn_2S_7^{6-}$ as inorganic ligands, and K-oleate as side product. DFT modeling combined with molecular dynamics, with or without inclusion of the polar solvent molecules into simulations (corresponding to colloidal or powdered state, respectively), confirms stable Cd-rich composition upon adsorption of $Sn_2S_7^{6-}$ or SnS_4^{4-} ligands. We note that NC compositions are very dynamic due to ligand adsorption−desorption equilibria and surface reconstruction. Furthermore, thiostannates SnS_4^{4-} and $Sn_2S_7^{6-}$ retain 4-coordinate Sn, despite the occurrence of significant distortions due to surface-binding. At the same time, experiments and simulations point to the instability of $Sn_2S_6^{4-}$ (and SnS_3^{2-}) in all studied solvents and its lower adaptability to the NC surface caused by rigid Sn_2S_2 rings. We suppose that the main observations of this study such as retention of metal-rich surfaces and X-type ligand exchange should be generally true for all strongly binding inorganic ligands such as chalcogenidometallates and metal-free chalcogenide ions. However, other inorganic ligand systems such as halometallates may exhibit different behaviors and should be studied in detail.

ASSOCIATED CONTENT

Supporting Information

File SI1 contains optimized geometries and input files for simulations. File SI2 contains Figures S1−S8, Tables S1−S2 and additional experimental details. This material is available free of charge via the Internet at http://pubs.acs.org.

AUTHOR INFORMATION

Corresponding Author

mvkovalenko@ethz.ch

Notes

The authors declare no competing financial interest.

ACKNOWLEDGMENTS

This work was financially supported by the European Union through FP7 (ERC Starting grant NANOSOLID, Grant No. 306733) and by ETH Zürich. Computations were performed on the GPC supercomputer at the SciNet HPC Consortium. SciNet is funded by the Canada Foundation for Innovation under the auspices of Compute Canada; the Government of Ontario; Ontario Research Fund—Research Excellence; and the University of Toronto. The Swiss Light Source (SLS) is thanked for provision of beamtime at the SuperXAS beamline. We acknowledge Dr. Ceri Hammond and Prof. Ive Hermans for the help with Raman measurements and Laura Piveteau for technical help during the revision of the manuscript.

REFERENCES

(1) (a) Talapin, D. V.; Lee, J.-S.; Kovalenko, M. V.; Shevchenko, E. V. *Chem. Rev.* **2009**, *110*, 389−458. (b) Murray, C. B.; Norris, D. J.; Bawendi, M. G. *J. Am. Chem. Soc.* **1993**, *115*, 8706−8715. (c) Yin, Y.; Alivisatos, A. P. *Nature* **2005**, *437*, 664−670.

(2) Guyot-Sionnest, P. *J. Phys. Chem. Lett.* **2012**, *3*, 1169−1175.

(3) (a) Kramer, I. J.; Sargent, E. H. *Chem. Rev.* **2013**, *114*, 863−882. (b) Gur, I.; Fromer, N. A.; Geier, M. L.; Alivisatos, A. P. *Science* **2005**, *310*, 462−465.

(4) (a) Anikeeva, P. O.; Halpert, J. E.; Bawendi, M. G.; Bulović, V. *Nano Lett.* **2007**, *7*, 2196−2200. (b) Caruge, J. M.; Halpert, J. E.; Wood, V.; Bulovic, V.; Bawendi, M. G. *Nat. Photonics* **2008**, *2*, 247−250.

(5) (a) Keuleyan, S.; Lhuillier, E.; Brajuskovic, V.; Guyot-Sionnest, P. *Nat. Photonics* **2011**, *5*, 489−493. (b) Clifford, J. P.; Konstantatos, G.; Johnston, K. W.; Hoogland, S.; Levina, L.; Sargent, E. H. *Nat. Nanotechnol.* **2009**, *4*, 40−44. (c) Jong-Soo, L.; Kovalenko, M. V.; Jing, H.; Dae Sung, C.; Talapin, D. V. *Nat. Nanotechnol.* **2011**, *6*, 348−352. (d) Sargent, E. H. *Adv. Mater.* **2008**, *20*, 3958−3964.

(6) (a) Kovalenko, M. V.; Spokoyny, B.; Lee, J.-S.; Scheele, M.; Weber, A.; Perera, S.; Landry, D.; Talapin, D. V. *J. Am. Chem. Soc.* **2010**, *132*, 6686−6695. (b) Ibanez, M.; Cadavid, D.; Zamani, R.; Garcia-Castello, N.; Izquierdo-Roca, V.; Li, W. H.; Fairbrother, A.; Prades, J. D.; Shavel, A.; Arbiol, J.; Perez-Rodriguez, A.; Morante, J. R.; Cabot, A. *Chem. Mater.* **2012**, *24*, 562−570. (c) Wang, R. Y.; Feser, J. P.; Lee, J.-S.; Talapin, D. V.; Segalman, R.; Majumdar, A. *Nano Lett.* **2008**, *8*, 2283−2288. (d) Ko, D.-K.; Kang, Y.; Murray, C. B. *Nano Lett.* **2011**, *11*, 2841−2844.

(7) Choi, J.-H.; Fafarman, A. T.; Oh, S. J.; Ko, D.-K.; Kim, D. K.; Diroll, B. T.; Muramoto, S.; Gillen, J. G.; Murray, C. B.; Kagan, C. R. *Nano Lett.* **2012**, *12*, 2631−2638.

(8) (a) Kim, D. K.; Lai, Y.; Diroll, B. T.; Murray, C. B.; Kagan, C. R. *Nat. Commun.* **2012**, *3*, 1216. (b) Koh, W. K.; Saudari, S. R.; Fafarman, A. T.; Kagan, C. R.; Murray, C. B. *Nano Lett.* **2011**, *11*, 4764−4767.

(9) (a) Kovalenko, M. V.; Scheele, M.; Talapin, D. V. *Science* **2009**, *324*, 1417−1420. (b) Kovalenko, M. V.; Bodnarchuk, M. I.; Zaumseil, J.; Lee, J.-S.; Talapin, D. V. *J. Am. Chem. Soc.* **2010**, *132*, 10085−10092.

(10) (a) Nag, A.; Kovalenko, M. V.; Lee, J.-S.; Liu, W.; Spokoyny, B.; Talapin, D. V. *J. Am. Chem. Soc.* **2011**, *133*, 10612−10620. (b) Ning, Z.; Dong, H.; Zhang, Q.; Voznyy, O.; Sargent, E. H. *ACS Nano* **2014**, *8*, 10321−10327. (c) Zhang, H.; Jang, J.; Liu, W.; Talapin, D. V. *ACS Nano* **2014**, *8*, 7359−7369. (d) Fafarman, A. T.; Koh, W. K.; Diroll, B. T.; Kim, D. K.; Ko, D. K.; Oh, S. J.; Ye, X. C.; Doan-Nguyen, V.; Crump, M. R.; Reifsnyder, D. C.; Murray, C. B.; Kagan, C. R. *J. Am. Chem. Soc.* **2011**, *133*, 15753−15761.

(11) (a) Llordes, A.; Hammack, A. T.; Buonsanti, R.; Tangirala, R.; Aloni, S.; Helms, B. A.; Milliron, D. J. *J. Mater. Chem.* **2011**, *21*, 11631−11638. (b) Llordes, A.; Garcia, G.; Gazquez, J.; Milliron, D. J. *Nature* **2013**, *500*, 323−326.

(12) Dirin, D. N.; Dreyfuss, S.; Bodnarchuk, M. I.; Nedelcu, G.; Papagiorgis, P.; Itskos, G.; Kovalenko, M. V. *J. Am. Chem. Soc.* **2014**, *136*, 6550−6553.

(13) (a) Doris, S. E.; Lynch, J. J.; Li, C.; Wills, A. W.; Urban, J. J.; Helms, B. A. *J. Am. Chem. Soc.* **2014**, *136*, 15702−15710. (b) Rosen, E. L.; Buonsanti, R.; Llordes, A.; Sawvel, A. M.; Milliron, D. J.; Helms, B. A. *Angew. Chem., Int. Ed.* **2012**, *51*, 684−689.

(14) (a) Lee, J.-S.; Kovalenko, M. V.; Huang, J.; Chung, D. S.; Talapin, D. V. *Nat. Nanotechnol.* **2011**, *6*, 348−352. (b) Chung, D. S.; Lee, J.-S.; Huang, J.; Nag, A.; Ithurria, S.; Talapin, D. V. *Nano Lett.* **2012**, *12*, 1813−1820. (c) Oh, S. J.; Berry, N. E.; Choi, J.-H.; Gaulding, E. A.; Lin, H.; Paik, T.; Hong, S.-H.; Murray, C. B.; Kagan, C. R. *ACS Nano* **2013**, *7*, 2413−2421. (d) Oh, S. J.; Berry, N. E.; Choi, J.-H.; Gaulding, E. A.; Lin, H.; Paik, T.; Diroll, B. T.; Muramoto, S.; Murray, C. B.; Kagan, C. R. *Nano Lett.* **2014**, *14*, 1559−1566. (e) Liu, W.; Lee, J.-S.; Talapin, D. V. *J. Am. Soc. Chem.* **2013**, *135*, 1349−1357. (f) Jang, J.; Liu, W.; Son, J. S.; Talapin, D. V. *Nano Lett.* **2014**, *14*, 653−662.

(15) (a) Munro, A. M.; Jen-La Plante, I.; Ng, M. S.; Ginger, D. S. *J. Phys. Chem. C* **2007**, *111*, 6220−6227. (b) Yakunin, S.; Dirin, D. N.; Protesescu, L.; Sytnyk, M.; Tollabimazraehno, S.; Humer, M.; Hackl, F.; Fromherz, T.; Bodnarchuk, M. I.; Kovalenko, M. V.; Heiss, W. *ACS Nano* **2014**, *8*, 12883−12894.

DOI: 10.1021/ja510862c
J. Am. Chem. Soc. 2015, 137, 1862−1874

(16) Nag, A.; Chung, D. S.; Dolzhnikov, D. S.; Dimitrijevic, N. M.; Chattopadhyay, S.; Shibata, T.; Talapin, D. V. *J. Am. Chem. Soc.* **2012**, *134*, 13604−13615.
(17) Kravchyk, K.; Protesescu, L.; Bodnarchuk, M. I.; Krumeich, F.; Yarema, M.; Walter, M.; Guntlin, C.; Kovalenko, M. V. *J. Am. Chem. Soc.* **2013**, *135*, 4199−4202.
(18) (a) Jiang, C.; Lee, J.-S.; Talapin, D. V. *J. Am. Chem. Soc.* **2012**, *134*, 5010−5013. (b) Liao, J. H.; Varotsis, C.; Kanatzidis, M. G. *Inorg. Chem.* **1993**, *32*, 2453−2462. (c) Ning, Z.; Voznyy, O.; Pan, J.; Hoogland, S.; Adinolfi, V.; Xu, J.; Li, M.; Kirmani, A. R.; Sun, J.-P.; Minor, J.; Kemp, K. W.; Dong, H.; Rollny, L.; Labelle, A.; Carey, G.; Sutherland, B.; Hill, I. G.; Amassian, A.; Liu, H.; Tang, J.; Bakr, O. M.; Sargent, E. H. *Nat. Mater.* **2014**, *13*, 822−828.
(19) Wang, R. Y.; Tangirala, R.; Raoux, S.; Jordan-Sweet, J. L.; Milliron, D. J. *Adv. Mater.* **2012**, *24*, 99−103.
(20) Kovalenko, M. V.; Schaller, R. D.; Jarzab, D.; Loi, M. A.; Talapin, D. V. *J. Am. Chem. Soc.* **2012**, *134*, 2457−2460.
(21) Gargas, D. J.; Chan, E. M.; Ostrowski, A. D.; Aloni, S.; Altoe, M. V. P.; Barnard, E. S.; Sanii, B.; Urban, J. J.; Milliron, D. J.; Cohen, B. E.; Schuck, P. J. *Nat. Nano* **2014**, *9*, 300−305.
(22) (a) Tang, J.; Kemp, K. W.; Hoogland, S.; Jeong, K. S.; Liu, H.; Levina, L.; Furukawa, M.; Wang, X.; Debnath, R.; Cha, D.; Chou, K. W.; Fischer, A.; Amassian, A.; Asbury, J. B.; Sargent, E. H. *Nat. Mater.* **2011**, *10*, 765−771. (b) Ning, Z.; Ren, Y.; Hoogland, S.; Voznyy, O.; Levina, L.; Stadler, P.; Lan, X.; Zhitomirsky, D.; Sargent, E. H. *Adv. Mater.* **2012**, *24*, 6295−6299. (c) Ip, A. H.; Thon, S. M.; Hoogland, S.; Voznyy, O.; Zhitomirsky, D.; Debnath, R.; Levina, L.; Rollny, L. R.; Carey, G. H.; Fischer, A.; Kemp, K. W.; Kramer, I. J.; Ning, Z.; Labelle, A. J.; Chou, K. W.; Amassian, A.; Sargent, E. H. *Nat. Nanotechnol.* **2012**, *7*, 577−582. (d) Katsiev, K.; Ip, A. H.; Fischer, A.; Tanabe, I.; Zhang, X.; Kirmani, A. R.; Voznyy, O.; Rollny, L. R.; Chou, K. W.; Thon, S. M.; Carey, G. H.; Cui, X.; Amassian, A.; Dowben, P.; Sargent, E. H.; Bakr, O. M. *Adv. Mater.* **2013**, *26*, 937−942. (e) Bae, W. K.; Joo, J.; Padilha, L. A.; Won, J.; Lee, D. C.; Lin, Q.; Koh, W.-K.; Luo, H.; Klimov, V. I.; Pietryga, J. M. *J. Am. Soc. Chem.* **2012**, *134*, 20160−20168. (f) Anderson, N. C.; Hendricks, M. P.; Choi, J. J.; Owen, J. S. *J. Am. Chem. Soc.* **2013**, *135*, 18536−18548. (g) Anderson, N. C.; Owen, J. S. *Chem. Mater.* **2013**, *25*, 69−76. (h) Owen, J. S.; Park, J.; Trudeau, P.-E.; Alivisatos, A. P. *J. Am. Chem. Soc.* **2008**, *130*, 12279−12281.
(23) (a) Chuang, C.-H. M.; Brown, P. R.; Bulović, V.; Bawendi, M. G. *Nat. Mater.* **2014**, *13*, 796−801. (b) Zhitomirsky, D.; Voznyy, O.; Levina, L.; Hoogland, S.; Kemp, K. W.; Ip, A. H.; Thon, S. M.; Sargent, E. H. *Nat. Commun.* **2014**, *5*, 3803.
(24) Voznyy, O.; Sargent, E. *Phys. Rev. Lett.* **2014**, *112*, 157401.
(25) Chen, O.; Chen, X.; Yang, Y.; Lynch, J.; Wu, H.; Zhuang, J.; Cao, Y. C. *Angew. Chem., Int. Ed.* **2008**, *47*, 8638−8641.
(26) (a) Larsen, F. H.; Skibsted, J.; Jakobsen, H. J.; Nielsen, N. C. *J. Am. Chem. Soc.* **2000**, *122*, 7080−7086. (b) Lefort, R.; Wiench, J. W.; Pruski, M.; Amoureux, J. P. *J. Chem. Phys.* **2002**, *116*, 2493−2501.
(27) Ravel, B.; Newville, M. *J. Synchrotron Radiat.* **2005**, *12*, 537−541.
(28) Zabinsky, S. I.; Rehr, J. J.; Ankudinov, A.; Albers, R. C.; Eller, M. J. *Phys. Rev. B* **1995**, *52*, 2995−3009.
(29) (a) Jasieniak, J.; Smith, L.; van Embden, J.; Mulvaney, P.; Califano, M. *J. Phys. Chem. C* **2009**, *113*, 19468−19474. (b) Yu, W. W.; Qu, L. H.; Guo, W. Z.; Peng, X. G. *Chem. Mater.* **2003**, *15*, 2854−2860.
(30) VandeVondele, J.; Krack, M.; Mohamed, F.; Parrinello, M.; Chassaing, T.; Hutter, J. *Comput. Phys. Commun.* **2005**, *167*, 103−128.
(31) Lippert, B. G.; Parrinello, J. H.; Michele. *Mol. Phys.* **1997**, *92*, 477−488.
(32) Hartwigsen, C.; Goedecker, S.; Hutter, J. *Phys. Rev. B* **1998**, *58*, 3641−3662.
(33) VandeVondele, J.; Hutter, J. *J. Chem. Phys.* **2007**, *127*, 114105.
(34) Voznyy, O.; Zhitomirsky, D.; Stadler, P.; Ning, Z.; Hoogland, S.; Sargent, E. H. *ACS Nano* **2012**, *6*, 8448−8455.
(35) Fritzinger, B.; Moreels, I.; Lommens, P.; Koole, R.; Hens, Z.; Martins, J. C. *J. Am. Chem. Soc.* **2009**, *131*, 3024−3032.
(36) Chen, O.; Yang, Y.; Wang, T.; Wu, H.; Niu, C.; Yang, J.; Cao, Y. C. *J. Am. Chem. Soc.* **2011**, *133*, 17504−17512.
(37) (a) Schiwy, V. B. k. u. W. *Z. Anorg. Allg. Chem.* **1973**, *63*−*71*, 398. (b) Krebs, B.; Pohl, S.; Schiwy, W. *Z. Anorg. Allg. Chem.* **1972**, *393*, 241−252. (c) Schiwy, W.; Pohl, S.; Krebs, B. *Z. Anorg. Allg. Chem.* **1973**, *402*, 77−86. (d) Krebs, B.; Pohl, S.; Schiwy, W. *Angew. Chem., Int. Ed.* **1970**, *9*, 897−898.
(38) Rangan, K. K.; Trikalitis, P. N.; Canlas, C.; Bakas, T.; Weliky, D. P.; Kanatzidis, M. G. *Nano Lett.* **2002**, *2*, 513−517.
(39) (a) Ruzin, E.; Zent, E.; Matern, E.; Massa, W.; Dehnen, S. *Chem.—Eur. J.* **2009**, *15*, 5230−5244. (b) Heine, J.; Dehnen, S. *Z. Anorg. Allg. Chem.* **2012**, *638*, 2425−2440.
(40) Manson, J. I. *Multinuclear NMR*; Plenum Publishing Corporation: New York, 1987; Vol. *1*.
(41) (a) Burns, R. C.; Devereux, L. A.; Granger, P.; Schrobilgen, G. J. *Inorg. Chem.* **1985**, *24*, 2615−2624. (b) Campbell, J.; Devereux, L. A.; Gerken, M.; Mercier, H. P. A.; Pirani, A. M.; Schrobilgen, G. J. *Inorg. Chem.* **1996**, *35*, 2945−2962. (c) Huffman, J. C.; Haushalter, J. P.; Umarji, A. M.; Shenoy, G. K.; Haushalter, R. C. *Inorg. Chem.* **1984**, *23*, 2312−2315. (d) Rudolph, R. W.; Wilson, W. L.; Taylor, R. C. *J. Am. Chem. Soc.* **1981**, *103*, 2480−2481. (e) Teller, R. G.; Krause, L. J.; Haushalter, R. C. *Inorg. Chem.* **1983**, *22*, 1809−1812. (f) Trikalitis, P. N.; Bakas, T.; Kanatzidis, M. G. *J. Am. Chem. Soc.* **2005**, *127*, 3910−3920. (g) *Multinuclear NMR*; Mason, J., Ed.; Plenum Press: New York, 1987.
(42) Mundus, C.; Taillades, G.; Pradel, A.; Ribes, M. *Solid State Nucl. Magn. Reson.* **1996**, *7*, 141−146.
(43) Gay, I. D.; Jones, C. H. W.; Sharma, R. D. *J. Magn. Reson.* **1989**, *84*, 501−514.
(44) (a) Pienack, N.; Naether, C.; Bensch, W. *Eur. J. Inorg. Chem.* **2009**, 937−946. (b) Yang, W.; Duan, H.-S.; Cha, K. C.; Hsu, C.-J.; Hsu, W.-C.; Zhou, H.; Bob, B.; Yang, Y. *J. Am. Chem. Soc.* **2013**, *135*, 6915−6920.
(45) Tomaselli, M.; Yarger, J. L.; Bruchez, M., Jr.; Havlin, R. H.; deGraw, D.; Pines, A.; Alivisatos, A. P. *J. Chem. Phys.* **1999**, *110*, 8861−8864.
(46) Berrettini, M. G.; Braun, G.; Hu, J. G.; Strouse, G. F. *J. Am. Chem. Soc.* **2004**, *126*, 7063−7070.
(47) (a) Blanc, F.; Coperet, C.; Lesage, A.; Emsley, L. *Chem. Soc. Rev.* **2008**, *37*, 518−526. (b) Reven, L. *J. Mol. Catal.* **1994**, *86*, 447−477.
(48) (a) Larsen, F. H.; Jakobsen, H. J.; Ellis, P. D.; Nielsen, N. C. *J. Phys. Chem. A* **1997**, *101*, 8597−8606. (b) Trebosc, J.; Wiench, J. W.; Huh, S.; Lin, V. S. Y.; Pruski, M. *J. Am. Chem. Soc.* **2005**, *127*, 7587−7593.
(49) Loyingood, D. D.; Achey, R.; Paravastu, A. K.; Strouse, G. F. *J. Am. Chem. Soc.* **2010**, *132*, 3344−3354.
(50) Hyun, B.-R.; Bartnik, A. C.; Koh, W.-k.; Agladze, N. I.; Wrubel, J. P.; Sievers, A. J.; Murray, C. B.; Wise, F. W. *Nano Lett.* **2011**, *11*, 2786−2790.
(51) Løver, T.; Bowmaker, G. A.; Seakins, J. M.; Cooney, R. P. *Chem. Mater.* **1997**, *9*, 967−975.
(52) (a) Tschirner, N.; Lange, H.; Schliwa, A.; Biermann, A.; Thomsen, C.; Lambert, K.; Gomes, R.; Hens, Z. *Chem. Mater.* **2012**, *24*, 311−318. (b) Kotkata, M. F.; Masoud, A. E.; Mohamed, M. B.; Mahmoud, E. A. *Physica E* **2009**, *41*, 640−645.
(53) Li, J. J.; Wang, Y. A.; Guo, W.; Keay, J. C.; Mishima, T. D.; Johnson, M. B.; Peng, X. *J. Am. Chem. Soc.* **2003**, *125*, 12567−12575.
(54) (a) Goel, R. G. *Spectrochim. Acta, Part A* **1981**, *37*, 557−558. (b) Jalilehvand, F.; Mah, V.; Leung, B. O.; Janos, M.; Bernard, G. M.; Laszlo, H. *Inorg. Chem.* **2009**, *48*, 4219−4230.
(55) Cordones, A. A.; Scheele, M.; Alivisatos, A. P.; Leone, S. R. *J. Am. Chem. Soc.* **2012**, *134*, 18366−18373.
(56) Puzder, A.; Williamson, A.; Gygi, F.; Galli, G. *Phys. Rev. Lett.* **2004**, *92*, 217401.

DOI: 10.1021/ja510862c
J. Am. Chem. Soc. 2015, 137, 1862−1874